Spin and diamagnetism in linear and nonlinear optics

Torsten Andersen,[1,2,*] Ole Keller,[3] Wolfgang Hübner,[2] and Börje Johansson[1]
[1]*CMT, Department of Physics, Ångström Laboratory, Uppsala University, Box 530, S-751 21 Uppsala, Sweden*
[2]*Department of Physics, Kaiserslautern University, Box 3049, D-67653 Kaiserslautern, Germany*
[3]*Institute of Physics, Aalborg University, Pontoppidanstræde 103, DK-9220 Aalborg Øst, Denmark*
(Received 4 March 2004; published 8 October 2004)

We present a local-field theory for spin and diamagnetism in linear and nonlinear optics. We examine all the processes contained in the Pauli Hamiltonian and its corresponding microscopic current density, including the terms depending on the electron spin. The resulting general real-space conductivities are presented and discussed. To quantify the implications of including the spin, we study the linear and nonlinear optical properties of free-electron metals, represented by the screened homogeneous electron gas. The real-space formalism is transformed into Fourier space, and the symmetries of the linear and nonlinear optical conductivities in a homogeneous electron gas are discussed. Numerical results are presented for the homogeneous electron gas, in which we treat ω and q as independent variables, thereby opening the theory to near-field optics and the study of evanescent waves. We show that in regions of the ω-q spectrum, the presence of diamagnetism and spin dynamics significantly alters the response in comparison to considering only the paramagnetic response. Additionally, we discuss the effects of screening, and we finish our treatment by a discussion of how to connect the present theory to existing methods in *ab initio* solid-state physics.

DOI: 10.1103/PhysRevA.70.043806 PACS number(s): 42.65.−k, 78.20.Bh, 51.70.+f

I. INTRODUCTION

The influence of the electron spin on the nonlinear optical response of condensed matter has to our knowledge so far only been described in connection with magnetism, surfaces, and interfaces. Experimental [1–13] as well as theoretical and numerical studies [12–21] have shown that the presence of magnetism leads to interesting and significant results. Dewitz, Chen, and Hübner [22,23] have performed a theoretical treatment of optical second-harmonic generation from magnetic thin films within the electric-dipole model, with focus on the use of density-functional theory (DFT) to determine the material properties. While providing a good starting point from a materials science point of view, the limitations of the electric-dipole model in the description of nonlinear optical responses from surfaces, interfaces, thin films, and even for the bulk in the presence of inversion symmetry, are well known [24]. It is therefore desirable to develop better theoretical models for the optics.

However, from an optical point of view, magnetism is a complicated phenomenon. It depends on the spin-orbit interaction and the exchange coupling, and it would be quite a complicated step to include everything into a model that both goes beyond the electric-dipole approximation and allows for inclusion of spin-dependent effects in a single-shot approach. In order to better understand the processes that are present in nonlinear optics, a better starting point would be to include the spin-dependent term from the Pauli Hamiltonian in the description, and limit the study to simpler metals.

In the present formulation we abandon from the outset some of the usually made approximations in optics, including (i) the concept of a refractive index, (ii) the local multipolar expansion (electric dipole, magnetic dipole, electric quadrupole, etc.), and (iii) the Born approximation. Abandoning the refractive-index concept is necessary if the theory should also be applicable to nonhomogeneous media, where large field gradients occur at, e.g., surfaces, interfaces, or impurities. Close to such features it would be impossible to tell exactly where to change from one refractive index to another. Thus it is more appropriate to allow the theoretical model to include such changes in a more direct manner, instead of attempting to modify the concept of the refractive index by, e.g., making it depend on spatial coordinates, wave vectors, time, etc. When the local dipole approximation becomes invalid (in both the inversion symmetric extreme of the bulk, and the extreme of nanostructures), one could resort to include the electric quadrupole, magnetic dipole, and higher-order terms, but it is difficult to determine where to terminate the multipolar expansion, and the analytical expressions become rather long. Those who might wish to derive the local multipoles can do so from our formalism using the Power-Zienau-Woolley transformation [31–33].

In any microscopic theory of the electromagnetic response one finds a nonlocal constitutive relation, where the response at one point $\boldsymbol{r}$ is related to the field-induced perturbations at neighboring points $\boldsymbol{r}'$ at earlier times. If the electromagnetic field is slowly varying over the neighboring points (for a metal, typically over a few atoms), the zeroth-order term of a Taylor series expansion of the electromagnetic field at $\boldsymbol{r}'$, $\boldsymbol{E}(\boldsymbol{r}';\omega)$, around $\boldsymbol{r}$ leads to the local approximation (see Ref. [29] for a detailed description). When the electromagnetic field varies rapidly, as is the case at interfaces or when evanescent fields are considered, the zeroth-order term of the Taylor series expansion becomes a rather poor approximation, and one thus has to go back to a nonlocal description.

Thus in Sec. II we develop expressions for the linear and second-harmonic nonlocal conductivity responses, starting

*Electronic address: thor@physik.uni-kl.de

from the microscopic Maxwell equations and the Pauli Hamiltonian. First, we introduce a gauge in order to describe the relation between the electric field and the vector potential, leading to a wave equation for the nonlinear optical response. In the construction of expressions for the relevant conductivities, the full Pauli Hamiltonian is considered, i.e., compared to conventional descriptions we include both the spin-dependent and the second-order terms of the interaction Hamiltonian, as well as the corresponding terms in the microscopic current density. Finally, we discuss the physical processes involved in the optical response. In Sec. III, we apply our theory for the spin conductivities to the homogeneous electron gas, paving the way for a numerical study of the influence of diamagnetism and spin on the optical response in the simplest possible system that can be described within a single-electron theory in the random-phase approximation. We establish the free-electron gas conductivity tensors in such a way that they obey the cylindrical symmetry around the optical axis. The resulting conductivities are compared to the Lindhard conductivities in terms of the so-called classical and quantum-mechanical nonlocality parameters in the sharp limit. We discuss the symmetries of the conductivities in the homogeneous electron gas, and finish the section by presenting and discussing numerical results with q and ω treated as independent variables (this is relevant for near-field optics and evanescent waves). The numerical results are focused on the free-electron properties of Cu. While the results in Sec. III are based on the local field, we look at the response to a transverse external electromagnetic field in Sec. IV. We begin this treatment by establishing the local-field loop for the propagation of an external electromagnetic (laser) field to the interaction region, and for the propagation of the response to the detector. In terms of the laser field and the field at the detector, we construct the relevant screened linear and nonlinear optical conductivities from (i) the conductivities we found for the local field and (ii) the screening processes. Numerical results for the screened linear and nonlinear conductivities are presented and discussed, and the section is finished with a discussion of the longitudinal and transverse collective resonances, the so-called *plasmons* and *plasmaritons*. In Sec. V, we discuss how to connect the present theory with existing numerical methods in *ab initio* condensed-matter physics, and, finally, in Sec. VI, we conclude.

II. DETERMINATION OF GENERAL LINEAR AND NONLINEAR SPIN CONDUCTIVITIES

We begin by analyzing Maxwells equations and choosing a particular gauge where the dynamical equations for the electric field and the vector potential are of the same form. Following this, we define a constitutive relation for the field-matter interaction, and establish a self-consistent loop for a monochromatic local electric field. Then we include the spin into the formalism of the Liouville equation of motion for the specific gauge and Hamiltonian we have chosen.

The resulting linear and nonlinear conductivities are especially well suited for (but not limited to) the description of (i) centrosymmetric materials, (ii) near-field optical processes of second order, and (iii) second-harmonic generation (SHG) processes in nanostructures such as quantum wells, quantum wires, quantum dots, clusters of atoms, molecules, etc.

A. Choice of gauge

The starting point for our electrodynamic analysis is the microscopic Maxwell-Lorentz equations, in which the material response at the space-time point $(\boldsymbol{r},t)$ is completely described via the microscopic current density $\boldsymbol{J}(\boldsymbol{r},t)$, and the related charge density, $\rho(\boldsymbol{r},t)$. If we denote the local electric and magnetic fields by $\boldsymbol{E}(\boldsymbol{r},t)$ and $\boldsymbol{B}(\boldsymbol{r},t)$, respectively, the microscopic field equations are

$$\boldsymbol{\nabla}\times\boldsymbol{E}(\boldsymbol{r},t)=-\frac{\partial\boldsymbol{B}(\boldsymbol{r},t)}{\partial t}, \tag{1}$$

$$\boldsymbol{\nabla}\times\boldsymbol{B}(\boldsymbol{r},t)=\mu_0\boldsymbol{J}(\boldsymbol{r},t)+\frac{1}{c_0^2}\frac{\partial\boldsymbol{E}(\boldsymbol{r},t)}{\partial t}, \tag{2}$$

$$\boldsymbol{\nabla}\cdot\boldsymbol{E}(\boldsymbol{r},t)=\frac{1}{\varepsilon_0}\rho(\boldsymbol{r},t), \tag{3}$$

$$\boldsymbol{\nabla}\cdot\boldsymbol{B}(\boldsymbol{r},t)=0, \tag{4}$$

where ε_0, μ_0, and $c_0=(\varepsilon_0\mu_0)^{-1/2}$ are the vacuum permittivity, permeability, and speed of light. To determine the local fields one needs in addition to the field equations, equations describing the response of the microscopic particles to the prevailing field. Here, only the electrons are assumed to be mobile, and their dynamics is described quantum mechanically on the basis of a single-particle approach. The starting point for our (nonrelativistic) calculation of the linear and nonlinear electron responses hence is the Pauli Hamiltonian

$$\mathcal{H}=\frac{1}{2m_e}[\boldsymbol{p}+e\boldsymbol{A}(\boldsymbol{r},t)]^2+\frac{e\hbar}{2m_e}\boldsymbol{\sigma}\cdot\boldsymbol{B}(\boldsymbol{r},t)-eU(\boldsymbol{r},t), \tag{5}$$

where m_e, $\boldsymbol{p}$, $-e$, and $\boldsymbol{\sigma}$ are the mass, conjugate momentum operator, charge, and spin operator of the electon, and $\hbar$ is Planck's constant divided by 2π. In the spin-field interaction term the g factor of the electron has been set to 2. In general it is not possible to eliminate the gauge dependent vector $[\boldsymbol{A}(\boldsymbol{r},t)]$ and scalar $[U(\boldsymbol{r},t)]$ potentials from the Hamiltonian in favor of the $\boldsymbol{E}$ and $\boldsymbol{B}$ fields. In the present context (see Sec. II C) it is adequate to make a particular gauge choice before carrying out, in a perturbative fashion, the calculation of the linear and nonlinear (second-harmonic) electron responses. Since the gauge we use is not the most common one, let us briefly consider the gauge choice and the resulting dynamical equations for $\mathbf{A}$ and U. The usual relations $\boldsymbol{B}(\boldsymbol{r},t)=\boldsymbol{\nabla}\times\boldsymbol{A}(\boldsymbol{r},t)$ and $\boldsymbol{E}(\boldsymbol{r},t)=-\partial\boldsymbol{A}(\boldsymbol{r},t)/\partial t-\boldsymbol{\nabla}U(\boldsymbol{r},t)$ ensure that the Maxwell equations (1) and (4) are automatically satisfied, and by insertion into the remaining inhomogeneous equations (2) and (3) one obtains the following coupled (standard) equations among $\boldsymbol{A}$ and U:

$$\Box\mathbf{A}(\boldsymbol{r},t)=\mu_0\boldsymbol{J}(\boldsymbol{r},t)-\boldsymbol{\nabla}\left[\boldsymbol{\nabla}\cdot\boldsymbol{A}(\boldsymbol{r},t)+\frac{1}{c_0^2}\frac{\partial U(\boldsymbol{r},t)}{\partial t}\right], \tag{6}$$

$$\Box U(\boldsymbol{r},t) = \frac{1}{\varepsilon_0}\rho(\boldsymbol{r},t) + \frac{\partial}{\partial t}\left[\boldsymbol{\nabla}\cdot\boldsymbol{A}(\boldsymbol{r},t) + \frac{1}{c_0^2}\frac{\partial U(\boldsymbol{r},t)}{\partial t}\right], \quad (7)$$

where $\Box = (1/c_0^2)\partial^2/\partial t^2 - \nabla^2$ is the d'Alembertian operator. In passing we would like to note for historical reasons that if the gauge choice of Lorenz [34,35], namely,

$$\boldsymbol{\nabla}\cdot\boldsymbol{A}(\boldsymbol{r},t) + \frac{1}{c_0^2}\frac{\partial U(\boldsymbol{r},t)}{\partial t} = 0, \quad (8)$$

is made the resulting wave equations for **A** and U, i.e., $\Box\boldsymbol{A} = \mu_0\boldsymbol{J}$ and $\Box U = \rho/\varepsilon_0$ couple only through the equation of continuity $\boldsymbol{\nabla}\cdot\boldsymbol{J} + \partial\rho/\partial t = 0$ (which is automatically fulfilled). These wave equations, which, together with Eq. (8), constitute a dynamical set of field equations completely analogous to the Maxwell equations were established in 1867 by L. V. Lorenz [34,35] independently of Maxwell. *The covariant form of the classical field equations hence was on the scene of physics in 1867*. The $\boldsymbol{E}$ and $\boldsymbol{B}$ fields are invariant under the gauge transformation

$$\boldsymbol{A}'(\boldsymbol{r},t) \rightarrow \boldsymbol{A}(\boldsymbol{r},t) = \boldsymbol{A}'(\boldsymbol{r},t) + \boldsymbol{\nabla}F(\boldsymbol{r},t), \quad (9)$$

$$U'(\boldsymbol{r},t) \rightarrow U(\boldsymbol{r},t) = U'(\boldsymbol{r},t) - \frac{\partial}{\partial t}F(\boldsymbol{r},t), \quad (10)$$

where F is an arbitrary function of $\boldsymbol{r}$ and t. If we divide the scalar potential into time-independent (0) and time-dependent (T) parts, i.e.,

$$U'(\boldsymbol{r},t) = U_0'(\boldsymbol{r}) + U_T'(\boldsymbol{r},t), \quad (11)$$

in this work we choose, starting from a general gauge, a gauge in which the time-dependent part of $U'(\boldsymbol{r},t)$ vanishes identically—that is,

$$\frac{\partial F(\boldsymbol{r},t)}{\partial t} = U_T'(\boldsymbol{r},t), \quad (12)$$

and therefore $U = U_0'(\boldsymbol{r}) = U_0(\boldsymbol{r})$. The dynamical equations for $\boldsymbol{A}(\boldsymbol{r},t)$ and $U_0(\boldsymbol{r})$ now take the forms

$$(\overleftrightarrow{\mathbb{1}}\Box + \boldsymbol{\nabla}\otimes\boldsymbol{\nabla})\cdot\boldsymbol{A}(\boldsymbol{r},t) = \mu_0\boldsymbol{J}(\boldsymbol{r},t), \quad (13)$$

$$\nabla^2 U_0(\boldsymbol{r}) = -\frac{1}{\varepsilon_0}\rho(\boldsymbol{r},t) - \frac{\partial}{\partial t}\boldsymbol{\nabla}\cdot\boldsymbol{A}(\boldsymbol{r},t), \quad (14)$$

where [in Eq. (13)] $\overleftrightarrow{\mathbb{1}}$ is the 3×3 unit tensor, and $\otimes$ is the dyadic (outer) product operator. In the gauge where the time-independent part of the scalar potential is set to zero the wave equation for $\boldsymbol{A}(\boldsymbol{r},t)$ does not contain $U = U_0(\boldsymbol{r})$. The differential equation in Eq. (14) which as it stands does contain both $\boldsymbol{A}$ and U_0 may be split into a time-independent part containing only U_0, viz.,

$$\nabla^2 U_0(\boldsymbol{r}) = -\frac{1}{\varepsilon_0}\rho_0(\boldsymbol{r}), \quad (15)$$

where $\rho_0(\boldsymbol{r})$ is the time-independent part of the microscopic charge density, and a time-dependent part $(1/\varepsilon_0)\rho_T(\boldsymbol{r},t) = -\partial\boldsymbol{\nabla}\cdot\boldsymbol{A}(\boldsymbol{r},t)/\partial t$ for $\boldsymbol{A}(\boldsymbol{r},t)$ [$\rho_T(\boldsymbol{r},t)$ being the time-varying part of ρ]. The equation for $\boldsymbol{A}(\boldsymbol{r},t)$ together with Eq. (13) ensures that the equation of continuity for the charge is always fulfilled. It is worth noting that the dynamical equations for $\boldsymbol{A}(\boldsymbol{r},t)$ in the gauge where the time-dependent part of the scalar potential is set to zero has the same form as the (usual) wave equation,

$$(\overleftrightarrow{\mathbb{1}}\Box + \boldsymbol{\nabla}\otimes\boldsymbol{\nabla})\cdot\boldsymbol{E}(\boldsymbol{r},t) = -\mu_0\frac{\partial\boldsymbol{J}(\boldsymbol{r},t)}{\partial t}, \quad (16)$$

for the microscopic electric field. By differentiation of Eq. (13) with respect to time, and subsequent use of $\partial\boldsymbol{A}(\boldsymbol{r},t)/\partial t = -\boldsymbol{E}(\boldsymbol{r},t) - \boldsymbol{\nabla}U_0(\boldsymbol{r})$ [and not just the incorrect $-\partial\boldsymbol{A}(\boldsymbol{r},t)/\partial t = \boldsymbol{E}(\boldsymbol{r},t)$!] one regains Eq. (16).

B. Wave equation for the nonlinear field

The generated nonlinear electric field of frequency 2ω is written as

$$\boldsymbol{E}_{\mathrm{NL}}(\boldsymbol{r},t) = \frac{1}{2}[\boldsymbol{E}_{\mathrm{NL}}(\boldsymbol{r};2\omega)e^{-i2\omega t} + \mathrm{c.c.}], \quad (17)$$

where "c.c." denotes the complex conjugate of the first term. In general, $\boldsymbol{E}(\boldsymbol{r},t)$ is a real quantity, i.e., $\boldsymbol{E}^*(\boldsymbol{r};\omega) = \boldsymbol{E}(\boldsymbol{r};-\omega)$. We will assume that the lowest-order nonlinear interaction dominates over higher-order mixing processes. Expanding the current density in a Fourier series in the incoming frequency, the relevant nonlinear current density is

$$\boldsymbol{J}_{\mathrm{NL}}(\boldsymbol{r},t) = \frac{1}{2}[\boldsymbol{J}_{\mathrm{NL}}(\boldsymbol{r};2\omega)e^{-i2\omega t} + \mathrm{c.c.}], \quad (18)$$

and the linear current density $\boldsymbol{J}_{\mathrm{L}}(\boldsymbol{r},t)$ is written in a similar manner. To account for the linear propagation of the second-harmonic response, the linear current density at 2ω contributes. Thus we retain the linear and the lowest-order nonlinear contribution. The wave equation for the second-harmonic response hence takes the form

$$\left[\overleftrightarrow{\mathbb{1}}\left(\frac{4\omega^2}{c_0^2} + \nabla^2\right) - \boldsymbol{\nabla}\otimes\boldsymbol{\nabla}\right]\cdot\boldsymbol{E}(\boldsymbol{r};2\omega) = -i2\mu_0\omega[\boldsymbol{J}_{\mathrm{L}}(\boldsymbol{r};2\omega) + \boldsymbol{J}_{\mathrm{NL}}(\boldsymbol{r};2\omega)]. \quad (19)$$

To close the self-consistent loop for the second-harmonic field, the microscopic current densities $\boldsymbol{J}_{\mathrm{L}}(\boldsymbol{r};2\omega)$ and $\boldsymbol{J}_{\mathrm{NL}}(\boldsymbol{r};2\omega)$ are given in terms of the local electric field through constitutive relations describing the field–matter interaction in a perturbative manner. The linear constitutive relation we write in the form

$$\boldsymbol{J}_{\mathrm{L}}(\boldsymbol{r};\omega) = \int \overleftrightarrow{\sigma}(\boldsymbol{r},\boldsymbol{r}';\omega)\cdot\boldsymbol{E}(\boldsymbol{r}';\omega)d^3r', \quad (20)$$

where $\overleftrightarrow{\sigma}(\boldsymbol{r},\boldsymbol{r}';\omega)$ is the linear conductivity tensor and the integration runs over the spatial interaction region. The ith element of the first-order current density is proportional to the integral of $[\overleftrightarrow{\sigma}\cdot\boldsymbol{E}]_i = \Sigma_j\sigma_{ij}E_j$. The second-order constitutive relation is written in a similar fashion, i.e.,

$$\boldsymbol{J}_{\mathrm{NL}}(\boldsymbol{r};2\omega)=\int\int \vec{\Sigma}(\boldsymbol{r},\boldsymbol{r}',\boldsymbol{r}'';\omega):\boldsymbol{E}(\boldsymbol{r}';\omega)\boldsymbol{E}(\boldsymbol{r}'';\omega)d^3r'd^3r'', \tag{21}$$

where $\vec{\Sigma}(\boldsymbol{r},\boldsymbol{r}',\boldsymbol{r}'';\omega)$ is the nonlocal second-order conductivity tensor. The two-dimensional sum–product operator ":" is here meant to be interpreted for the ith element of the second-harmonic current density as $[\vec{\Sigma}:\boldsymbol{EE}]_i=\Sigma_{jk}\Sigma_{ijk}E_jE_k$, i.e., i is the resulting coordinate (corresponds to the unprimed variables), j corresponds to the single-primed variables, and k to the double-primed variables. The electric fields appearing in Eqs. (20) and (21) can in general be different from each other. Inserting Eqs. (20) and (21) into Eq. (19) the loop for the second-harmonic field is closed.

C. Spin-dependent Hamiltonian

The starting point for this calculation is the Liouville equation of motion for the single-particle density-matrix operator ρ, i.e.,

$$i\hbar\frac{\partial\rho}{\partial t}=[\mathcal{H},\rho]. \tag{22}$$

In the equation above, the single-particle Pauli Hamiltonian $\mathcal{H}$ appearing in the commutator $[\mathcal{H},\rho]$ in the present description is given by

$$\mathcal{H}(\boldsymbol{r},t)=\mathcal{H}_0(\boldsymbol{r})+\mathcal{H}_{\mathrm{I}}(\boldsymbol{r},t)+\mathcal{H}_{\mathrm{R}}, \tag{23}$$

where $\mathcal{H}_0$ is the nonrelativistic (Schrödinger) Hamiltonian operator for the electron in the material when the perturbing optical field is absent, $\mathcal{H}_{\mathrm{I}}$ is the electron-photon interaction Hamiltonian, and $\mathcal{H}_{\mathrm{R}}$ represents the irreversible coupling to the "surroundings." $\mathcal{H}_0(\boldsymbol{r})=(1/2m_e)\boldsymbol{p}\cdot\boldsymbol{p}+V(\boldsymbol{r})$, where V is the potential energy of the electron, viz. $V=-eU$.

Introducing the vector potential as a sum of two Fourier components, i.e.,

$$\boldsymbol{A}(\boldsymbol{r},t)=\frac{1}{2}\boldsymbol{A}(\boldsymbol{r};\omega)e^{-i\omega t}+\text{c.c.}, \tag{24}$$

we divide the interaction Hamiltonian according to the different optical (electron-photon) processes it describes, i.e.,

$$\mathcal{H}_{\mathrm{I}}(\boldsymbol{r},t)=\frac{1}{2}\{[\mathcal{H}_1(\boldsymbol{r};\omega)+\mathcal{H}_1^{\sigma}(\boldsymbol{r};\omega)]e^{-i\omega t}+\text{H.a.}\}+\mathcal{H}_2^0(\boldsymbol{r})+\frac{1}{2}[\mathcal{H}_2(\boldsymbol{r};2\omega)e^{-i2\omega t}+\text{H.a.}], \tag{25}$$

where $\mathcal{H}_1$ is the part of the interaction Hamiltonian that is linear in the vector potential $\boldsymbol{A}(\boldsymbol{r},t)$ and independent of the spin, $\mathcal{H}_1^{\sigma}$ is the spin-dependent part of the interaction Hamiltonian, $\mathcal{H}_2$ is the interaction Hamiltonian of second order in $\boldsymbol{A}(\boldsymbol{r},t)$, "H.a." denotes the Hermitian adjoint. The Hermitian adjoint is found from the relation $[\mathcal{H}(\boldsymbol{r};\omega)]^{\dagger}=\mathcal{H}(\boldsymbol{r};-\omega)$ for any part of the interaction Hamiltonian, where † stands for Hermitian adjugation [36]. Hence the linear interaction terms read [38]

$$\mathcal{H}_1(\boldsymbol{r};\omega)=\frac{e}{2m_e}[\boldsymbol{p}\cdot\boldsymbol{A}(\boldsymbol{r};\omega)+\boldsymbol{A}(\boldsymbol{r};\omega)\cdot\boldsymbol{p}], \tag{26}$$

$$\mathcal{H}_1^{\sigma}(\boldsymbol{r};\omega)=\mu_{\mathrm{B}}\boldsymbol{\sigma}\cdot\boldsymbol{B}(\boldsymbol{r};\omega) \tag{27}$$

and the nonlinear interaction terms are

$$\mathcal{H}_2^0(\boldsymbol{r})=\frac{e^2}{4m_e}\boldsymbol{A}(\boldsymbol{r};\omega)\cdot\boldsymbol{A}(\boldsymbol{r};-\omega), \tag{28}$$

$$\mathcal{H}_2(\boldsymbol{r};2\omega)=\frac{e^2}{4m_e}\boldsymbol{A}(\boldsymbol{r};\omega)\cdot\boldsymbol{A}(\boldsymbol{r};\omega), \tag{29}$$

where $\mu_{\mathrm{B}}=e\hbar/(2m_e)$ is the Bohr magneton. For a spin-1/2 particle, such as the electron, the three Cartesian components of the Pauli spin operator can be represented by the Pauli spin matrices (the so-called standard representation)

$$\sigma_x=\begin{pmatrix}0&1\\1&0\end{pmatrix},\quad \sigma_y=\begin{pmatrix}0&-i\\i&0\end{pmatrix},\quad \sigma_z=\begin{pmatrix}1&0\\0&-1\end{pmatrix}, \tag{30}$$

taking the z axis as the quantization axis.

D. Mean current density

For the sake of interpretational simplicity it is appropriate to choose a basis where spin and space coordinates are separated. Considering the spin (without spin-orbit and exchange interactions, and neglecting correlation effects as well) response we make use of a spinor representation of the eigenfunctions of the field-unperturbed Hamiltonian, i.e., $|n,s\rangle=|n\rangle\otimes|s\rangle$, and in the $\boldsymbol{r}$ representation, we may write

$$\langle\boldsymbol{r}|n,s\rangle=\langle\boldsymbol{r}|n\rangle\otimes|s\rangle \tag{31}$$

with $\psi_n(\boldsymbol{r})=\langle\boldsymbol{r}|n\rangle$, and where we have used the fact that the eigenenergies are degenerate for our particular $\mathcal{H}_0$. Thus $|n\rangle$ and $|s\rangle$ are orthogonal. The Schrödinger equation is then

$$\mathcal{H}_0(\boldsymbol{r})|n,s\rangle=\mathcal{E}_n|n,s\rangle, \tag{32}$$

and for any operator O that separates into a product of a space-dependent and a spin-dependent term, i.e., $O=O_rO_{\sigma}$ we may thus write

$$\langle n,s|O|n',s'\rangle=\langle n|O_r|n'\rangle\langle s|O_{\sigma}|s'\rangle. \tag{33}$$

Consequently, the matrix representation of $\mathcal{H}_0$ is diagonal ($\langle n,s|\mathcal{H}_0|n',s'\rangle=\mathcal{E}_n\delta_{nn'}\delta_{ss'}$), and

$$\langle n,s|[\mathcal{H}_0,\rho]|n',s'\rangle=(\mathcal{E}_n-\mathcal{E}_{n'})\langle n|\rho_r|n'\rangle\langle s|\rho_{\sigma}|s'\rangle. \tag{34}$$

Introducing the usual transition frequency $\omega_{nn'}=(\mathcal{E}_n-\mathcal{E}_{n'})/\hbar$, the solution to the Liouville equation becomes $\langle n|\rho_0(\boldsymbol{r},t)|n'\rangle=f_n\langle n|n'\rangle\delta_{nn'}$, since the thermal excitation is expected to be an incoherent process, and therefore cannot produce coherent superpositions of atomic states ($\langle n|\rho_0(\boldsymbol{r})|n'\rangle=0$ for $n\neq n'$). It is thus called the thermal equilibrium density matrix, which for a fermion (such as the electron) is given by the Fermi-Dirac distribution for thermodynamic equilibrium, i.e.,

$$\langle a|\rho_0(\boldsymbol{r})|a\rangle \equiv f_a = \left[1 + \exp\left(\frac{\mathcal{E}_a - \mu}{k_B T}\right)\right]^{-1} \tag{35}$$

for state a (a is n' or n above), k_B being the Boltzmann constant, μ the chemical potential of the electron system, and T the absolute temperature.

As often is the practice in optics we assume that the irreversible coupling to the surrounding reservoir can be described using a phenomenological relaxation-time ansatz in the Liouville equation, so that

$$\frac{1}{i\hbar}\langle n|[\mathcal{H}_R, \rho(\boldsymbol{r},t)]|n'\rangle = \frac{\langle n|\rho_0(\boldsymbol{r})|n'\rangle - \langle n|\rho(\boldsymbol{r},t)|n'\rangle}{\tau_{nn'}}, \tag{36}$$

$n \neq n'$. It is convenient to expand the density matrix in a power series in the form $\rho(\boldsymbol{r},t) = \rho_0(\boldsymbol{r}) + \Sigma_{\alpha=1}^{\infty}\rho_\alpha(\boldsymbol{r},t)$, where α represents the number of incoming photons. The quantity $\tau_{nn'}$ in Eq. (36) is the relaxation time associated with the nn'th density matrix element. It is in general depending on both the electron momentum and spin [39,40]. Thus in order to describe the different second-order processes we need only the three lowest orders in the power series. The density matrix depends, of course, on the electron spin, so it is convenient to write $\rho_1(\boldsymbol{r},t)$ and $\rho_2(\boldsymbol{r},t)$ in terms of the spin, as well as in terms of a Fourier series in the frequency of the incoming field in the manner

$$\rho_1(\boldsymbol{r},t) = \frac{1}{2}\{[\rho_1(\boldsymbol{r};\omega) + \rho_1^\sigma(\boldsymbol{r};\omega)]e^{-i\omega t} + \text{H.a.}\}, \tag{37}$$

$$\rho_2(\boldsymbol{r},t) = \rho_2^0(\boldsymbol{r}) + \frac{1}{2}\{[\rho_2(\boldsymbol{r};2\omega) + \rho_2^\sigma(\boldsymbol{r};2\omega) + \rho_2^{\sigma\sigma}(\boldsymbol{r};2\omega)]e^{-i2\omega t} + \text{H.a.}\}. \tag{38}$$

By knowledge of the matrix elements $\langle n|\rho_0(\boldsymbol{r})|m\rangle$ we may find the matrix elements of the terms of higher order in the power series expansion of the density matrix in the usual iterative manner.

In order to determine the conductivity response tensors, $\overleftrightarrow{\sigma}(\boldsymbol{r},\boldsymbol{r}';\omega)$ and $\overleftrightarrow{\Sigma}(\boldsymbol{r},\boldsymbol{r}',\boldsymbol{r}'';\omega)$, appropriate for describing the second-order processes, we consider the ensemble average $\boldsymbol{J}(\boldsymbol{r},t)$ of the microscopic single-particle current-density operator $\boldsymbol{j}(\boldsymbol{r},t)$. This ensemble average is obtained as the trace of $\rho\boldsymbol{j}$, carried out in the usual manner as a quantum-mechanical double sum over states, i.e.,

$$\boldsymbol{J}(\boldsymbol{r},t) = \text{Tr}\{\rho(\boldsymbol{r},t)\boldsymbol{j}(\boldsymbol{r},t)\} \equiv \sum_{nn'ss'}\langle n,s|\rho(\boldsymbol{r},t)|n',s'\rangle\langle n',s'|\boldsymbol{j}(\boldsymbol{r},t)|n,s\rangle. \tag{39}$$

The microscopic current density $\boldsymbol{j}(\boldsymbol{r},t)$, as well as the transition matrix elements between two quantum states can be found in Appendix A.

E. Linear spin conductivity

For the ease of understanding it is favorable to divide the direct (unscreened) linear optical conductivity tensor into four parts, according to the different optical processes they describe, i.e., into the following parts:

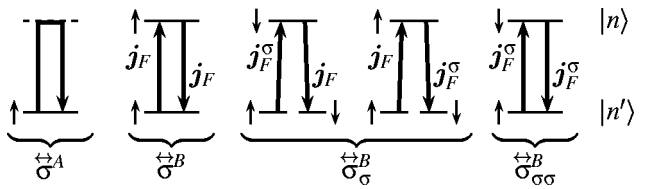

FIG. 1. Linear optical processes. The leftmost process is diamagnetic and does thus not change the spin configuration. The second process from the left is the usual paramagnetic process, and it does not change the spin configuration. The next two processes from the left change the spin configuration once during the process, and thus the spin configuration of the ground state. The rightmost process flips the spin twice during the process, and does not change the spin configuration of the ground state.

$$\overleftrightarrow{\sigma} = \overleftrightarrow{\sigma}^A + \overleftrightarrow{\sigma}^B + \overleftrightarrow{\sigma}^B_\sigma + \overleftrightarrow{\sigma}^B_{\sigma\sigma}, \tag{40}$$

where the subscript σ indicates the number of spin transition current densities contained in the conductivity tensor. The different optical processes involved in creating the total linear current density are shown schematically in Fig. 1. Omitting the spin terms, the division is the usual one, and with our particular basis and $\mathcal{H}_0$, $\overleftrightarrow{\sigma}^B_\sigma$ is identically zero (the basis and Hamiltonian does not allow the ground-state spin of the electron to change). An explicit calculation has confirmed that this is true after carrying out the spin summation. The linear current density is to be obtained from

$$\boldsymbol{J}_L(\boldsymbol{r};\omega) = \text{Tr}\{\rho_0\boldsymbol{j}_1\} + \text{Tr}\{\rho_1\boldsymbol{j}_F\} + \text{Tr}\{\rho_1^\sigma\boldsymbol{j}_F^\sigma\}, \tag{41}$$

where the different microscopic currents are given in Appendix A. The three terms in Eq. (41) above are the diamagnetic, paramagnetic, and spin terms, respectively. After a tedious but straightforward insertion of the relevant expressions, followed by execution of the spin summation, we find that the three corresponding parts of the linear conductivity tensor are

$$\overleftrightarrow{\sigma}^A(\boldsymbol{r},\boldsymbol{r}';\omega) = \frac{2ie^2}{\omega m_e}\sum_n f_n\langle n|\delta(\boldsymbol{r}' - \boldsymbol{r}_e)|n\rangle\overleftrightarrow{\mathbb{1}}\delta(\boldsymbol{r} - \boldsymbol{r}'), \tag{42}$$

$$\overleftrightarrow{\sigma}^B(\boldsymbol{r},\boldsymbol{r}';\omega) = \frac{2i}{\hbar\omega}\sum_{nn'}\frac{f_n - f_{n'}}{\omega_{nn'} - \omega - i/\tau_{nn'}} \times\langle n'|\boldsymbol{j}_F(\boldsymbol{r})|n\rangle \otimes \langle n|\boldsymbol{j}_F(\boldsymbol{r}')|n'\rangle, \tag{43}$$

and

$$\overleftrightarrow{\sigma}^B_{\sigma\sigma}(\boldsymbol{r},\boldsymbol{r}';\omega) = \frac{2i}{\hbar\omega}\sum_{nn'}\frac{f_n - f_{n'}}{\omega_{nn'} - \omega - i/\tau_{nn'}}[\overleftrightarrow{\mathbb{1}}\langle n'|\boldsymbol{j}_F^s(\boldsymbol{r})|n\rangle \cdot \langle n|\boldsymbol{j}_F^s(\boldsymbol{r}')|n'\rangle - \langle n|\boldsymbol{j}_F^s(\boldsymbol{r}')|n'\rangle \otimes \langle n'|\boldsymbol{j}_F^s(\boldsymbol{r})|n\rangle], \tag{44}$$

respectively [consult Ref. [41], Eq. (3.113)].

The diamagnetic part of the linear conductivity tensor [Eq. (42)] has the symmetry of the unit tensor appearing in it,

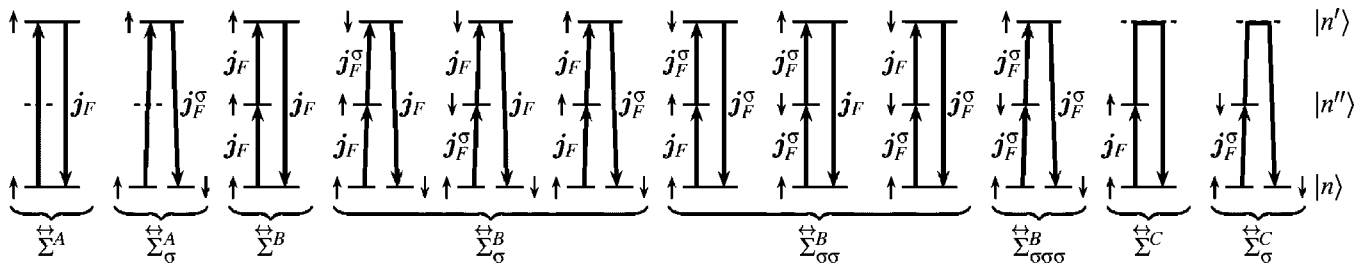

FIG. 2. Possible nonlinear optical processes when spin is included consistently in the formalism. The division is done according to the number of spin flips involved in each process and the different orders of the processes. Under the braces is mentioned which part each process corresponds to in Eq. (45). The two leftmost and the two rightmost processes are partly diamagnetic, while the rest contains different combinations of the free current (spin-dependent as well as spin-independent part).

and thus three nonzero elements in the diagonal which are all equal to each other. The two other linear conductivities have in general nine nonzero independent elements. In order to reduce the number of tensor elements, one can specialize the treatment to specific systems, which we shall see in Sec. III.

F. Nonlinear spin conductivity

It is favorable to divide the total direct (unscreened) nonlinear optical conductivity tensor into separate parts according to the different optical processes that appear when one takes the trace involved in generating the nonlinear current density, i.e., we get

$$\overleftrightarrow{\Sigma} = \overleftrightarrow{\Sigma}^A + \overleftrightarrow{\Sigma}^A_\sigma + \overleftrightarrow{\Sigma}^B + \overleftrightarrow{\Sigma}^B_\sigma + \overleftrightarrow{\Sigma}^B_{\sigma\sigma} + \overleftrightarrow{\Sigma}^B_{\sigma\sigma\sigma} + \overleftrightarrow{\Sigma}^C + \overleftrightarrow{\Sigma}^C_\sigma, \quad (45)$$

which by omission of the spin reduces to the division made in previous works [42]. The nonlinear current density is obtained as

$$\begin{aligned} \boldsymbol{J}_{\mathrm{NL}}(\boldsymbol{r};2\omega) = {} & \mathrm{Tr}\{\rho_2 \boldsymbol{j}_F\} + \mathrm{Tr}\{\rho_2 \boldsymbol{j}_F^\sigma\} + \mathrm{Tr}\{\rho_2^\sigma \boldsymbol{j}_F\} + \mathrm{Tr}\{\rho_2^\sigma \boldsymbol{j}_F^\sigma\} \\ & + \mathrm{Tr}\{\rho_2^{\sigma\sigma} \boldsymbol{j}_F\} + \mathrm{Tr}\{\rho_2^{\sigma\sigma} \boldsymbol{j}_F^\sigma\} + \frac{1}{2}\mathrm{Tr}\{\rho_1 \boldsymbol{j}_1\} \\ & + \frac{1}{2}\mathrm{Tr}\{\rho_1^\sigma \boldsymbol{j}_1\}. \end{aligned} \quad (46)$$

The different optical processes involved in creating the nonlinear current density are sketched in Fig. 2. The traces correspond to the nonlinear conductivity tensors as follows: The first trace contains the processes appearing in $\overleftrightarrow{\Sigma}^A$ and $\overleftrightarrow{\Sigma}^B$. The second trace contains the process appearing in $\overleftrightarrow{\Sigma}^A_\sigma$ and the rightmost process of $\overleftrightarrow{\Sigma}^B_\sigma$ in Fig. 2. The third trace describes the two other processes in $\overleftrightarrow{\Sigma}^B_\sigma$. The fourth trace contains the leftmost and the rightmost processes of $\overleftrightarrow{\Sigma}^B_{\sigma\sigma}$ as depicted in Fig. 2, and the fifth trace contains the centermost process there. The sixth trace represents the process in $\overleftrightarrow{\Sigma}^B_{\sigma\sigma\sigma}$. The seventh trace corresponds to $\overleftrightarrow{\Sigma}^C$, and the eighth to $\overleftrightarrow{\Sigma}^C_\sigma$. It is easy to show (by carrying out the spin summation) that with our particular basis and $\mathcal{H}_0$ all tensor parts with an odd number of spins are zero.

The processes that end in another spin configuration than they begin in are only possible if the Hamiltonian allows for them, e.g., by (i) an inclusion of terms that allow for different spin populations in the ground state, such as the spin-orbit interaction and the exchange coupling, or (ii) include two-electron processes where one electron goes from one spin state to the other at the same time as another electron goes the other way. The latter point is excluded by the choice of a single-electron theory. Including either of the above-mentioned features will result in the fact that all processes in Fig. 2 should be considered, and additional new processes would have to be taken into account, since more processes than those described here become possible.

Thus the nonlinear spin conductivity can be identified as $\overleftrightarrow{\Sigma}^B_{\sigma\sigma}$ alone. With a little algebra, ending, as in the linear case, with performing the spin summation, the nonzero nonlinear conductivity tensors can be identified as

$$\overleftrightarrow{\Sigma}^A(\boldsymbol{r},\boldsymbol{r}',\boldsymbol{r}'';\omega) = \frac{i}{4\hbar\omega^2}\frac{e^2}{m_e}\sum_{nn'}\frac{f_{n'}-f_n}{\omega_{nn'}-2\omega-i/\tau_{nn'}}\langle n'|\boldsymbol{j}_F(\boldsymbol{r})|n\rangle \otimes \overleftrightarrow{\mathbb{1}}\langle n|\delta(\boldsymbol{r}'-\boldsymbol{r}_e)|n'\rangle\delta(\boldsymbol{r}'-\boldsymbol{r}''), \quad (47)$$

$$\begin{aligned} \overleftrightarrow{\Sigma}^B(\boldsymbol{r},\boldsymbol{r}',\boldsymbol{r}'';\omega) = {} & -\frac{1}{\omega^2\hbar^2}\sum_{nn'n''}\frac{1}{\omega_{nn'}-2\omega-i/\tau_{nn'}}\left(\frac{f_n-f_{n''}}{\omega_{nn''}-\omega-i/\tau_{nn''}}-\frac{f_{n''}-f_{n'}}{\omega_{n''n'}-\omega-i/\tau_{n''n'}}\right)\langle n'|\boldsymbol{j}_F(\boldsymbol{r})|n\rangle \otimes \langle n''|\boldsymbol{j}_F(\boldsymbol{r}')|n'\rangle \\ & \otimes \langle n|\boldsymbol{j}_F(\boldsymbol{r}'')|n''\rangle, \end{aligned} \quad (48)$$

TABLE I. An overview of which terms contribute to which tensor element of $\vec{\vec{\Sigma}}^{B}_{\sigma\sigma}$. The first column lists the different indices j and k, the second to fourth columns list the different contributions to elements with $i=x$, $i=y$, and $i=z$, respectively. In the latter three columns, abbreviations have been used in the following way: A bar over a symbol indicates that it is a component of a matrix element of the spin-independent transition current density $\boldsymbol{j}_F$, taken in the Cartesian direction of the symbol, i.e., along x, y, or z. The others (without bars) are components of a matrix element of the spin-dependent transition current density $\boldsymbol{j}^s_F$, with the same rule as before. The primes refer to the index of the spatial coordinates $\boldsymbol{r}$, $\boldsymbol{r}'$, and $\boldsymbol{r}''$, respectively. As can be observed from this table, no two tensor elements have moduli equal to each other in the general case.

jk	$i=x$ contains	$i=y$ contains	$i=z$ contains
xx	$\overline{xz}'z''+\overline{xy}'y''+zz'\overline{x}''+yy'\overline{x}''+yx'\overline{y}''+zx'\overline{z}''$	$\overline{yz}'z''+\overline{yy}'y''-xy'\overline{x}''-xx'\overline{y}''$	$\overline{zz}'z''+\overline{zy}'y''-xz'\overline{x}''-xx'\overline{z}''$
xy	$-\overline{xy}'x''+zz'\overline{y}''+yy'\overline{y}''-yx'\overline{x}''$	$-\overline{yy}'x''-xy'\overline{y}''+xx'\overline{x}''+zx'\overline{z}''$	$-\overline{zy}'x''-xz'\overline{y}''-yx'\overline{z}''$
xz	$-\overline{xz}'x''+zz'\overline{z}''+yy'\overline{z}''-zx'\overline{x}''$	$-\overline{yz}'x''-xy'\overline{z}''-zx'\overline{y}''$	$-\overline{zz}'x''-xz'\overline{z}''+xx'\overline{x}''+yx'\overline{y}''$
yx	$-\overline{xx}'y''-yx'\overline{x}''+yy'\overline{y}''+zy'\overline{z}''$	$-\overline{yx}'y''+zz'\overline{x}''+xx'\overline{x}''-xy'\overline{y}''$	$-\overline{zx}'y''-yz'\overline{x}''-xy'\overline{z}''$
yy	$\overline{xz}'z''+\overline{xx}'x''-yx'\overline{x}''-yy'\overline{x}''$	$\overline{yz}'z''+\overline{yx}'x''+zz'\overline{y}''+xx'\overline{y}''+xy'\overline{x}''+zy'\overline{z}''$	$\overline{zz}'z''+\overline{zx}'x''-yz'\overline{y}''-yy'\overline{z}''$
yz	$-\overline{xz}'y''-yx'\overline{z}''-zy'\overline{x}''$	$-\overline{yz}'y''+zz'\overline{z}''+xx'\overline{z}''-zy'\overline{y}''$	$-\overline{zz}'y''-yz'\overline{z}''+xy'\overline{x}''+yy'\overline{y}''$
zx	$-\overline{xx}'z''-zx'\overline{x}''+yz'\overline{z}''+zz'\overline{z}''$	$-\overline{yx}'z''-zy'\overline{x}''-xz'\overline{y}''$	$-\overline{zx}'z''+xx'\overline{x}''+yy'\overline{x}''-xz'\overline{z}''$
zy	$-\overline{xy}'z''-zx'\overline{y}''-yz'\overline{x}''$	$-\overline{yy}'z''-zy'\overline{y}''+xz'\overline{x}''+zz'\overline{z}''$	$-\overline{zy}'z''+xx'\overline{y}''+yy'\overline{y}''-yz'\overline{z}''$
zz	$\overline{xx}'x''+\overline{xy}'y''-zx'\overline{z}''-zz'\overline{x}''$	$\overline{yx}'x''+\overline{yy}'y''-zy'\overline{z}''-zz'\overline{y}''$	$\overline{zx}'x''+\overline{zy}'y''+xx'\overline{z}''+yy'\overline{z}''+xz'\overline{x}''+yz'\overline{y}''$

$$\vec{\vec{\Sigma}}^{B}_{\sigma\sigma}(\boldsymbol{r},\boldsymbol{r}',\boldsymbol{r}'';\omega)=-\frac{1}{\omega^2\hbar^2}\sum_{nn'n''}\frac{1}{\omega_{nn'}-2\omega-i/\tau_{nn'}}\left(\frac{f_n-f_{n''}}{\omega_{nn''}-\omega-i/\tau_{nn''}}-\frac{f_{n''}-f_{n'}}{\omega_{n''n'}-\omega-i/\tau_{n''n'}}\right)$$
$$\times\{\langle n'|\boldsymbol{j}_F(\boldsymbol{r})|n\rangle\otimes(\vec{\vec{1}}\langle n''|\boldsymbol{j}^s_F(\boldsymbol{r}')|n'\rangle\cdot\langle n|\boldsymbol{j}^s_F(\boldsymbol{r}'')|n''\rangle-\langle n|\boldsymbol{j}^s_F(\boldsymbol{r}'')|n''\rangle\otimes\langle n''|\boldsymbol{j}^s_F(\boldsymbol{r}')|n'\rangle)+(\vec{\vec{1}}\langle n'|\boldsymbol{j}^s_F(\boldsymbol{r})|n\rangle\cdot\langle n''|\boldsymbol{j}^s_F(\boldsymbol{r}')|n'\rangle$$
$$-\langle n''|\boldsymbol{j}^s_F(\boldsymbol{r}')|n'\rangle\otimes\langle n'|\boldsymbol{j}^s_F(\boldsymbol{r})|n\rangle)\otimes\langle n|\boldsymbol{j}_F(\boldsymbol{r}'')|n''\rangle+\langle n'|\boldsymbol{j}^s_F(\boldsymbol{r})|n\rangle\cdot\langle n|\boldsymbol{j}^s_F(\boldsymbol{r}'')|n''\rangle\sum_{i\in\{x,y,z\}}\boldsymbol{e}_i\otimes\langle n''|\boldsymbol{j}_F(\boldsymbol{r}')|n'\rangle\otimes\boldsymbol{e}_i$$
$$-\langle n|\boldsymbol{j}^s_F(\boldsymbol{r}'')|n''\rangle\otimes\langle n''|\boldsymbol{j}_F(\boldsymbol{r}')|n'\rangle\otimes\langle n'|\boldsymbol{j}^s_F(\boldsymbol{r})|n\rangle\}, \tag{49}$$

$$\vec{\vec{\Sigma}}^{C}(\boldsymbol{r},\boldsymbol{r}',\boldsymbol{r}'';\omega)=-\frac{1}{\hbar\omega^2}\frac{e^2}{m_e}\sum_{nn'}\frac{f_n-f_{n'}}{\omega_{nn'}-\omega-i/\tau_{nn'}}\langle n'|\delta(\boldsymbol{r}-\boldsymbol{r}_e)|n\rangle\vec{\vec{1}}\otimes\langle n|\boldsymbol{j}_F(\boldsymbol{r}'')|n'\rangle\delta(\boldsymbol{r}-\boldsymbol{r}'). \tag{50}$$

Whereas the three spin-independent terms of the nonlinear conductivity tensor have quite intuitive structures in terms of simple outer products, the spin-dependent one [Eq. (49)] is more complicated in its structure (because of the spin summation), with a mixture of inner and outer products between transition current densities. Therefore an overview of the different contributions to each of the 27 generally independent Cartesian components of the nonlinear spin-dependent conductivity tensor is given in Table I.

Looking at Eqs. (47)–(50) one observes that part B [Eq. (48)] and the spin part [Eq. (49)] of the nonlinear conductivity tensor in the general case have 27 nonzero and independent elements. Part A [Eq. (47)] has, due to the appearance of the 3×3 unit tensor, nine nonzero elements, of which only three are independent, since elements with indices $jk\in\{xx,yy,zz\}$ are equal. Similarly, and for the same reason, part C [Eq. (50)] has nine nonzero elements, of which three are independent but here it is elements with indices $ij\in\{xx,yy,zz\}$ that are equal.

Reduction of the number of nonzero independent elements can be done in many ways by selecting different physical systems to investigate, i.e., by applying a specific set of symmetries and translational invariance (discrete or continuous). The simplest possible system leading to a nonzero result is the homogeneous electron gas, which we hence will discuss in the following.

III. SPIN CONDUCTIVITY IN A HOMOGENEOUS ELECTRON GAS

A. Translational invariance

In the homogeneous three-dimensional electron gas (3DEG), there is translational invariance in all three dimensions, and at $q=0$ it is also inversion symmetric. Thus the conductivity tensors become functions of the relative distances between coordinates rather than the coordinates themselves, i.e., $\vec{\vec{\sigma}}(\boldsymbol{r},\boldsymbol{r}')\to\vec{\vec{\sigma}}(\boldsymbol{r}-\boldsymbol{r}')$, and $\vec{\vec{\Sigma}}(\boldsymbol{r},\boldsymbol{r}',\boldsymbol{r}'')\to\vec{\vec{\Sigma}}(\boldsymbol{r}-\boldsymbol{r}',\boldsymbol{r}-\boldsymbol{r}'')$. The presence of a finite $\boldsymbol{q}$ breaks the inversion symmetry and thus allows for nonlinear optical processes to take place.

The translational invariance in all three dimensions makes it natural to express the various vector and tensor quantities

in a Fourier representation. Thus, for any vector field $\boldsymbol{V}$,

$$\boldsymbol{V}(\boldsymbol{r};\omega) = \frac{1}{(2\pi)^3}\int \boldsymbol{V}(\boldsymbol{q},\omega)e^{i\boldsymbol{q}\cdot\boldsymbol{r}}d^3q. \tag{51}$$

In the three-dimensional Fourier representation the relevant constitutive relations take the forms

$$\boldsymbol{J}_{\mathrm{L}}(\boldsymbol{q},\omega) = \overleftrightarrow{\sigma}(\boldsymbol{q},\omega)\cdot\boldsymbol{E}(\boldsymbol{q},\omega) \tag{52}$$

and

$$\boldsymbol{J}_{\mathrm{NL}}(2\boldsymbol{q},2\omega) = \frac{1}{(2\pi)^3}\overleftrightarrow{\Sigma}(2\boldsymbol{q},\omega):\boldsymbol{E}(\boldsymbol{q},\omega)\boldsymbol{E}(\boldsymbol{q},\omega), \tag{53}$$

respectively, where we have imposed the conditions for second-harmonic generation, i.e., (i) the two incoming fields have the same wave vector, called $\boldsymbol{q}$, and (ii) the generated second-harmonic field has the wave vector $2\boldsymbol{q}$.

It is convenient also to express the wave function $\psi_n(\boldsymbol{r})$ as a Fourier series over all possible values of the wave vector. The basis set for the space-dependent part of the wave function may thus be taken in the form

$$\psi_{\boldsymbol{k}_n}(\boldsymbol{r}) = \frac{1}{(2\pi)^{3/2}}e^{i\boldsymbol{k}_n\cdot\boldsymbol{r}}, \tag{54}$$

where $\boldsymbol{k}$ is a real quantity. In both Eqs. (51) and (54) we have normalized the periodic function for later convenience.

The space-dependent transition current density from state n' to state n ($\langle n,s|\boldsymbol{j}_F(\boldsymbol{r})|n',s'\rangle = \langle n|\boldsymbol{j}_F(\boldsymbol{r})|n'\rangle\delta_{ss'}$), takes, by means of Eq. (54), the form

$$\langle n|\boldsymbol{j}_F(\boldsymbol{r})|n'\rangle = -\frac{1}{(2\pi)^3}\frac{e\hbar}{2m_e}(\boldsymbol{k}_{n'}+\boldsymbol{k}_n)e^{i(\boldsymbol{k}_{n'}-\boldsymbol{k}_n)\cdot\boldsymbol{r}}, \tag{55}$$

in a notation where adequate subscripts have been added to the wave vectors. Similarly, the spin-dependent transition current density becomes

$$\langle n|\boldsymbol{j}_F^{\mathrm{S}}(\boldsymbol{r})|n'\rangle = -\frac{1}{(2\pi)^3}\frac{ie\hbar}{2m_e}(\boldsymbol{k}_{n'}-\boldsymbol{k}_n)e^{i(\boldsymbol{k}_{n'}-\boldsymbol{k}_n)\cdot\boldsymbol{r}}. \tag{56}$$

Finally,

$$\langle n|\delta(\boldsymbol{r}-\boldsymbol{r}_e)|n\rangle = \frac{1}{(2\pi)^3}, \tag{57}$$

and we should mention that the Fermi-Dirac distribution function and the transition frequencies become $\boldsymbol{k}$ dependent, i.e., since the eigenenergy takes the form

$$\mathcal{E}_n = \frac{\hbar^2}{2m_e}|\boldsymbol{k}_n|^2, \tag{58}$$

we find

$$f_n \equiv f_n(\boldsymbol{k}_n) = f_n\left(\frac{\hbar^2}{2m_e}|\boldsymbol{k}_n|^2\right) \tag{59}$$

and

$$\omega_{nn'} = \frac{\hbar}{2m_e}(|\boldsymbol{k}_n|^2 - |\boldsymbol{k}_{n'}|^2). \tag{60}$$

The latter quantity we will denote $\omega_{nn'}(\boldsymbol{k}_n,\boldsymbol{k}_{n'})$ in the following, for brevity.

B. Linear spin conductivity and its relation to the Lindhard conductivities

In the three-dimensional Fourier space one can construct relevant direct linear conductivity tensors by combining Eqs. (20), (51), and (52), giving

$$\overleftrightarrow{\sigma}(\boldsymbol{q},\omega) = \frac{1}{(2\pi)^3}\int \overleftrightarrow{\sigma}(\boldsymbol{R};\omega)e^{-i\boldsymbol{q}\cdot\boldsymbol{R}}d^3R, \tag{61}$$

$\boldsymbol{R}=\boldsymbol{r}-\boldsymbol{r}'$, from which the individual parts of the nonlinear conductivity tensor are then calculated by (i) successive insertion of the relevant conductivity tensor part and Eqs. (55)–(57), (ii) integration over the $\boldsymbol{r}$ spaces, (iii) assume that different $\boldsymbol{k}$'s spans a three-dimensional continuum, thereby allowing us to reduce the number of $\boldsymbol{k}$'s to one by integration and thus remove the remaining index on it, since it is thereafter superfluous, (iv) reorientation of the space in the direction of $\boldsymbol{q}$, i.e., $\boldsymbol{q}=q\boldsymbol{e}_x$, and (v) since we are working with a quite simple basis, it also makes sense to reduce our expressions to what they will be for a free-electron gas in the low-temperature limit [43], and a single relaxation time τ. After a little algebra, the expressions for the linear space conductivity tensors in a 3DEG appear as

$$\overleftrightarrow{\sigma}^{\mathrm{A}}(q,\omega) = \frac{2ie^2}{\omega m_e}\int \Theta(\boldsymbol{k})\frac{d^3k}{(2\pi)^3}\overleftrightarrow{\mathbb{1}}, \tag{62}$$

$$\overleftrightarrow{\sigma}^{\mathrm{B}}(q,\omega) = \frac{ie^2\hbar}{2m_e^2\omega}\int \frac{\Theta(\boldsymbol{k}+q\boldsymbol{e}_x)-\Theta(\boldsymbol{k})}{\hbar(q^2+2k_xq)/2m_e-\omega-i/\tau} \times(2\boldsymbol{k}+q\boldsymbol{e}_x)\otimes(2\boldsymbol{k}+q\boldsymbol{e}_x)\frac{d^3k}{(2\pi)^3}, \tag{63}$$

and the spin conductivity,

$$\overleftrightarrow{\sigma}^{\mathrm{B}}_{\sigma\sigma}(q,\omega) = \frac{ie^2\hbar q^2}{2m_e^2\omega}\int \frac{\Theta(\boldsymbol{k}+q\boldsymbol{e}_x)-\Theta(\boldsymbol{k})}{\hbar(q^2+2k_xq)/2m_e-\omega-i/\tau}\frac{d^3k}{(2\pi)^3} \times[\overleftrightarrow{\mathbb{1}}-\boldsymbol{e}_x\otimes\boldsymbol{e}_x], \tag{64}$$

in integral form [compare Eqs. (62) and (63) to Ref. [30]].

Equations (62) and (63) are the famous Lindhard conductivities [44]. Refined spatial conductivities that let the electron system relax towards local thermal equilibrium can be established [45]. A similar refinement can be done for the spin conductivity.

The analytical solution to these integrals is discussed in Appendix B. Above, we observe (i) that $\lim_{\boldsymbol{q}\to 0}\overleftrightarrow{\sigma}^{\mathrm{B}}_{\sigma\sigma}(\boldsymbol{q},\omega) = \overleftrightarrow{0}$, and (ii) that the last term in $\overleftrightarrow{\sigma}^{\mathrm{B}}_{\sigma\sigma}(\boldsymbol{q},\omega)$ projects out the transverse electric field, since $\boldsymbol{E}_T\perp\boldsymbol{q}$. This is a remarkable feature of the spin conductivity, since both the diamagnetic and the paramagnetic conductivities contribute to both the longitudinal and the transverse electric fields.

Performing the integration over $\boldsymbol{k}$ space (see Appendix C), the longitudinal $[\sigma_{\mathrm{L}}(q,\omega)=\sigma^{A}(q,\omega)+\sigma^{B}_{xx}(q,\omega)]$ and transverse $[\sigma_{\mathrm{T}}(q,\omega)=\sigma^{A}(q,\omega)+\sigma^{B}_{yy}(q,\omega)]$ linear conductivities appear in the usual [29,44,46–48] manner in the sharp limit $(\tau\to\infty)$ as

$$\sigma_{\mathrm{L}}(q,\omega)=\frac{3e^2nu^2}{2im_e\omega}\left[1+\frac{1}{4z}\left(\left[1-(u-z)^2\right]\ln\left|\frac{z-u+1}{z-u-1}\right|+\left[1-(u+z)^2\right]\ln\left|\frac{z+u+1}{z+u-1}\right|\right)\right], \tag{65}$$

$$\sigma_{T}(q,\omega)=\frac{3ie^2n}{8m_e\omega}\left[z^2+3u^2+1-\frac{1}{4z}\left(\left[1-(u-z)^2\right]^2\ln\left|\frac{z-u+1}{z-u-1}\right|+\left[1-(u+z)^2\right]^2\ln\left|\frac{z+u+1}{z+u-1}\right|\right)\right], \tag{66}$$

where $n=k_F^3/3\pi^2$, $u=\omega/qv_F$ and $z=q/2k_F$ are the "classical" and "quantum-mechanical" nonlocality parameters, respectively, and $v_F=\hbar k_F/m_e$ is the Fermi velocity of the electron. In the same representation, the linear spin conductivity becomes

$$\sigma^{B}_{\sigma\sigma}(q,\omega)=\frac{3e^2nz^2}{2im_e\omega}\left[1+\frac{1}{4z}\left(\left[1-(u-z)^2\right]\ln\left|\frac{z-u+1}{z-u-1}\right|+\left[1-(u+z)^2\right]\ln\left|\frac{z+u+1}{z+u-1}\right|\right)\right]. \tag{67}$$

Peculiarly (since it is transverse), the expression for the spin conductivity is very similar to the longitudinal conductivity. One observes that

$$\sigma^{B}_{\sigma\sigma}(q,\omega)=\frac{z^2}{u^2}\sigma_{\mathrm{L}}(q,\omega). \tag{68}$$

The factor by which the spin conductivity differs from the longitudinal conductivity is $z/u=\hbar q^2/2\omega m_e$ squared, and at $q=q_0=\omega/c_0$, we find that $\hbar\omega=2m_ec_0^2$ is the photon energy required to make the spin conductivity of the same size as the longitudinal conductivity. That is two times the rest mass energy of the electron! The nonrelativistic description we are using is assumed to be valid only for $\hbar\omega\ll m_ec_0^2$. Thus, for $q=q_0$, the spin contribution to the linear response is vanishing. If, however, we look at q and ω as independent variables (which they can be viewed as in configurations with large contributions from evanescent waves), we observe that for large values of q and small values of ω, $z\gg u$, and the spin contribution is dominating. This we shall substantiate on in a separate communication.

C. Nonlinear spin conductivity

In the three-dimensional Fourier space one can construct relevant direct nonlinear conductivity tensors by combining Eqs. (21), (51), and (53), giving the general expression

$$\overleftrightarrow{\Sigma}(2\boldsymbol{q},\omega)=\frac{1}{(2\pi)^3}\int\int\Sigma(\boldsymbol{R},\boldsymbol{R}';\omega)e^{-i\boldsymbol{q}\cdot(\boldsymbol{R}+\boldsymbol{R}')}d^3R'd^3R, \tag{69}$$

$\boldsymbol{R}=\boldsymbol{r}-\boldsymbol{r}'$ and $\boldsymbol{R}'=\boldsymbol{r}-\boldsymbol{r}''$. Performing this convolution integral, one actually obtains a nonlinear conductivity tensor that depends on two generally different $\boldsymbol{q}$'s. Let us call them $\boldsymbol{q}$ and $\boldsymbol{q}'$. In our particular case we are interested in the second-harmonic response, and we choose $\boldsymbol{q}=\boldsymbol{q}'$. From Eq. (69), the individual parts of the nonlinear conductivity tensor are then calculated using a procedure analogous to that of the linear conductivity, i.e., by (i) successive insertion of the relevant conductivity tensor part and Eqs. (55)–(57), (ii) integration over the $\boldsymbol{r}$ spaces, (iii) assume that the different $\boldsymbol{k}$'s spans a three-dimensional continuum, (iv) reorienting the space in the direction of $\boldsymbol{q}$, (v) take a free-electron gas in the low-temperature limit [43], and a single relaxation time τ, and (vi) taking into account the permutation symmetry between indices j and k that exist due to the single incoming electric field. Thus we get

$$\overleftrightarrow{\Sigma}^{A}(2q;2\omega)=\frac{e^3}{4m_e^2\omega^2}\int\frac{\Theta(\boldsymbol{k}+2q\boldsymbol{e}_x)-\Theta(\boldsymbol{k})}{2\hbar(q^2+k_xq)/m_e-2\omega-i/\tau}\times(\boldsymbol{k}+q\boldsymbol{e}_x)\otimes\overleftrightarrow{1}\frac{d^3k}{(2\pi)^3}, \tag{70}$$

$$\overleftrightarrow{\Sigma}^{B}(2q;2\omega)=\frac{e^3\hbar}{8m_e^3\omega^2}\int\frac{1}{2\hbar k_xq/m_e-2\omega-i/\tau}\left(\frac{\Theta(\boldsymbol{k}+q\boldsymbol{e}_x)-\Theta(\boldsymbol{k})}{\hbar(q^2+2k_xq)/2m_e-\omega-i/\tau}-\frac{\Theta(\boldsymbol{k})-\Theta(\boldsymbol{k}-q\boldsymbol{e}_x)}{\hbar\left(2k_xq-q^2\right)/2m_e-\omega-i/\tau}\right)\times\boldsymbol{k}\otimes\left[(2\boldsymbol{k}+q\boldsymbol{e}_x)\otimes(2\boldsymbol{k}-q\boldsymbol{e}_x)+(2\boldsymbol{k}-q\boldsymbol{e}_x)\otimes(2\boldsymbol{k}+q\boldsymbol{e}_x)\right]\frac{d^3k}{(2\pi)^3}, \tag{71}$$

$$\overleftrightarrow{\Sigma}^{B}_{\sigma\sigma}(2q;2\omega)=\frac{e^3\hbar q^2}{4m_e^3\omega^2}\int\frac{1}{2\hbar k_xq/m_e-2\omega-i/\tau}\left(\frac{\Theta(\boldsymbol{k}+q\boldsymbol{e}_x)-\Theta(\boldsymbol{k})}{\hbar(q^2+2k_xq)/2m_e-\omega-i/\tau}-\frac{\Theta(\boldsymbol{k})-\Theta(\boldsymbol{k}-q\boldsymbol{e}_x)}{\hbar\left(2k_xq-q^2\right)/2m_e-\omega-i/\tau}\right)\times\sum_{i\in\{y,z\}}(\boldsymbol{e}_i\otimes\boldsymbol{e}_i\otimes\boldsymbol{k}+\boldsymbol{e}_i\otimes\boldsymbol{k}\otimes\boldsymbol{e}_i-\boldsymbol{k}\otimes\boldsymbol{e}_i\otimes\boldsymbol{e}_i)\frac{d^3k}{(2\pi)^3}, \tag{72}$$

$$\overleftrightarrow{\Sigma}^{C}(2q;2\omega)=\frac{e^3}{4m_e^2\omega^2}\int\frac{\Theta(\boldsymbol{k}+q\boldsymbol{e}_x)-\Theta(\boldsymbol{k})}{\hbar(q^2+2k_xq)/2m_e-\omega-i/\tau}\sum_{i\in\{x,y,z\}}[\boldsymbol{e}_i\otimes\boldsymbol{e}_i\otimes(2\boldsymbol{k}+q\boldsymbol{e}_x)+\boldsymbol{e}_i\otimes(2\boldsymbol{k}+q\boldsymbol{e}_x)\otimes\boldsymbol{e}_i]\frac{d^3k}{(2\pi)^3}. \quad (73)$$

It should be noted here that Eqs. (71) and (72) each have other representations that in view of Eq. (53) lead to the same physically observable second-harmonic field, but their self-symmetry is lower. In contrast, Eq. (73) has a representation with higher self-symmetry—but in order to make the nonlinear conductivity tensor represent the overall cylindrical symmetry, the lower-symmetry representation above has been chosen [compare Eqs. (70), (71), and (73) to the expressions given in Ref. [49]]. The analytical solution to the integrals appearing in Eqs. (70)–(73) is discussed in Appendix B.

The above-mentioned response functions [Eqs. (62)–(64) and (70)–(73)] can also be used in the description of a semi-infinite medium [49], but the Friedel oscillations [50] are lost.

D. Symmetries of the nonlocal conductivity tensors

Part A of the linear conductivity tensor [Eq. (62)] is diagonal, i.e., $xx=yy=zz$, part B [Eq. (63)] has two independent nonzero elements, namely xx and $yy=zz$, and the linear spin conductivity tensor [Eq. (64)] reflects the fact that it projects out the transverse part, i.e., it has one independent nonzero element, $yy=zz$. These symmetries are shown in Fig. 3. We observe from Fig. 3 that the linear spin conductivity *cannot* be separated in a measurement, not even differentially. The reason being that in the total linear conductivity there are two nonzero elements, namely (i) the one coupling longitudinal input polarization to longitudinal output, $\sigma_{xx}=\sigma^A+\sigma^B_{xx}$, and (ii) the other one that couples transverse input polarization to transverse output, $\sigma_{yy}=\sigma^A+\sigma^B_{yy}+\sigma^B_{\sigma\sigma}$. The result is that we end up with two coupled equations with four unknowns, making separation impossible.

Letting $\boldsymbol{q}\|\boldsymbol{e}_x$, we recognize immediately the fact that in order to give nonzero contributions, the nonlinear conductivity tensors have to be even in y, as well as in z, reducing the number of possible nonzero elements from 27 to 7, namely the elements xxx, xyy, xzz, yyx, yxy, zzx, zxz.

With this selection, throughout the rest of the paper we will use the terms *longitudinal* and *transverse* electromagnetic fields, where a longtitudinal field is parallel to $\boldsymbol{e}_x$, and a transverse field is perpendicular to $\boldsymbol{e}_x$. In a cylindrically symmetric system this distinction is the logical and minimal one.

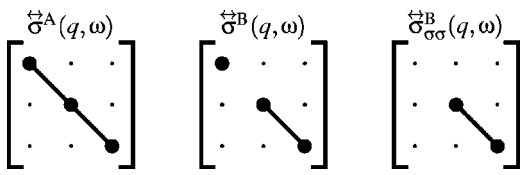

FIG. 3. Self-symmetries of the linear nonlocal conductivity tensor, each column corresponding to one tensor part, as shown. The dots represent elements with zero moduli, while the disks represent elements with nonzero moduli. Lines connect tensor elements of equal nonzero moduli.

Diamagnetic part A of the nonlinear space conductivity contributes purely to the longitudinal response, and contributes evenly to this response, no matter which input polarization is chosen. It does that via the three nonzero elements, $xxx=xyy=xzz$, that are equal due to the unit tensor appearing in the outer product of Eq. (70). It is depicted in the symmetry scheme Fig. 4(a).

The paramagnetic part B of the nonlinear conductivity [given by Eq. (71)] has seven nonzero tensor elements, of which two are independent, since the y and z directions are equivalent. The independent element xxx is the one that couples longitudinal input polarization to longitudinal output polarization. The other independent element, $xyy=xzz=yxy=yyx=zxz=zzx$, is responsible for coupling transverse input to longitudinal output, as well as mixed input to transverse output. These properties are shown in Fig. 4(b).

The contributions from the nonlinear spin conductivity can be identified by the terms appearing in the parentheses appearing after the sum in Eq. (72). The first term contributes to elements yyx and zzx, the second term contributes to elements yxy and zxz, and the third term contributes to elements xyy and xzz, giving a total of six nonzero tensor elements. As

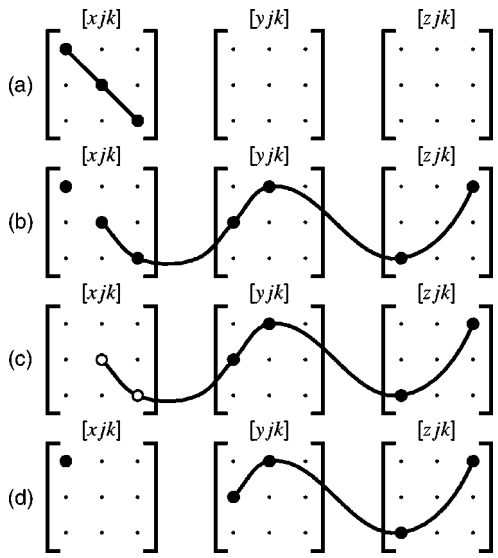

FIG. 4. Self-symmetries of the nonlocal nonlinear conductivity tensor, each row corresponding to one tensor part, and each column to a Cartesian coordinate in the second-harmonic field. Row (a) corresponds to $\overleftrightarrow{\Sigma}^{A}(2q,2\omega)$, row (b) to $\overleftrightarrow{\Sigma}^{B}(2q,2\omega)$, row (c) to $\overleftrightarrow{\Sigma}^{B}_{\sigma\sigma}(2q,2\omega)$, and row (d) to $\overleftrightarrow{\Sigma}^{C}(2q,2\omega)$. Elements with equal nonzero moduli are connected with lines, a dot represents an element with zero modulus, disks represent elements with nonzero modulus, and open circles represent elements with equal moduli as the disks they are connected to, but they have opposite sign.

can be seen from Eq. (72), the term in front of the sum is the same for all elements, and inside the sum appear only unit vectors and $\boldsymbol{k}=k\boldsymbol{e}_x$. Thus all six tensor elements have the same magnitude, but as can be seen from the signs, elements *xyy* and *xzz* have opposite sign from the others. This is illustrated in Fig. 4(c), and we notice in particular that the spin conductivity *does not* contribute to the pure longitudinal process (it has no *xxx* element), as in the linear case.

Finally, the diamagnetic part C of the nonlinear conductivity contributes to two types of processes through its two different nonzero elements. Looking at Eq. (73), we observe that it contributes to the pure longitudinal process with an *xxx* element, and to the process with mixed input polarization and transverse output polarization through the element $yxy=yyx=zxz=zzx$. The two different nonzero elements are related by a factor of 2, i.e., $\Sigma^C_{xxx}/2=\Sigma^C_{yxy}$. The resulting symmetry scheme is depicted in Fig. 4(d).

We observe from Fig. 4 that no element of any of the individual parts of the nonlinear conductivity can be measured independently. However, unlike in the linear case, this nonseparability can be broken by differential measurements. This is so, because it is possible to measure three elements of the total nonlinear conductivity independently, namely using the following optical configurations: (i) longitudinal input polarization with longitudinal response gives $\Sigma_{xxx}=\Sigma^A+\Sigma^B_{xxx}+\Sigma^C_{xxx}$, (ii) transverse input polarization with longitudinal response gives $\Sigma_{xyy}=\Sigma^A+\Sigma^B_{xyy}-\Sigma^B_{\sigma\sigma}$, and (iii) mixed transverse and longitudinal input polarization with a transverse response gives us $\Sigma_{yxy}=\Sigma^B_{yxy}+\Sigma^B_{\sigma\sigma}+\Sigma^C_{yxy}$. Adding to that the fact that we know the relation $\Sigma^C_{xxx}/2=\Sigma^C_{yxy}$, we end up with three equations with three unknowns, from which we in principle can extract each of the nonzero elements in Fig. 4. Of course, in order to be able to do this, we need both the amplitude and phase information.

E. Spin conductivities with q and ω as independent variables

The integrals appearing in Eqs. (62)–(64) and (70)–(73) can be solved analytically. The solution is discussed in some detail in Appendixes B and C. In order to calculate the direct [52] linear and nonlinear optical conductivities, we still need to determine the Fermi wave number k_F. In a 3DEG, it is $k_F=\sqrt[3]{3\pi^2\mathcal{N}}$ [see, e.g., Ref. [53], Eq. (2.21)], where $\mathcal{N}$ is the free-electron density of the 3DEG.

1. Linear conductivity

The moduli of the different elements contributing to the linear nonlocal conductivity are plotted in Figs. 5(a)–5(d), while the moduli of the two independent elements of the complete (sum of all terms) linear conductivity are plotted in Figs. 5(e) and 5(f). In all plots we are varying the two independent variables occurring in Eqs. (62)–(64), namely the cyclic frequency of the incoming photons in units of the photon energy $\hbar\omega$, and the wave number q in units of the Fermi wave number k_F. All calculations have been performed with the electron density and relaxation time of Cu ($\mathcal{N}=8.47\times10^{28}$ m^{-3}, $\tau=27$ fs, giving $k_F=1.36$ Å^{-1} [53]). The phase information has been left out here and in subsequent figures for brevity. Since linear and nonlinear optical processes usually are able to resolve many orders of magnitude in the optical response, all figures have been plotted on a logarithmic scale. To guide the eye, contours are plotted at every integer order of magnitude, and a line at the bottom of each figure denotes the position of the vacuum wave number $q=q_0=\omega/c_0$.

Figure 5(a) naturally reflects the fact that the diamagnetic linear conductivity [as given by Eq. (62)] does not depend on q. Figures 5(b) and 5(c) show the two independent nonzero elements of the paramagnetic linear conductivity, σ^B_{xx} and σ^B_{yy}, respectively [consult Eq. (63)]. They are roughly of the same order of magnitude, but the longitudinal one (σ^B_{xx}) falls off a bit slower than the transverse one (σ^B_{yy}), as ω increases. In Fig. 5(d), the linear spin conductivity shows the expected, generally much lower, order of magnitude compared to both the diamagnetic and the paramagnetic conductivities in the region of large ω and small q. In the region with small ω and large values of q, however, it is the dominating contribution to the total linear conductivity [compare Eqs. (63) and (64)].

Additionally, we observe that there is a region in the ω-q space where the paramagnetic conductivity has a larger magnitude than the diamagnetic conductivity, and regions where it is opposite. This is illustrated in Fig. 5(e) and 5(f), whereas the spin conductivity, as expected, leaves no easily recognizable mark on the total linear conductivity in the greater part of the ω-q space. Only in the corner where q is large and ω small, the order of magnitude of the spin conductivity becomes larger than competing components. Figure 5(e) is the longitudinal conductivity, $\sigma_{xx}=\sigma^A+\sigma^B_{xx}$, and (f) the transverse conductivity, $\sigma_{yy}=\sigma^A+\sigma^B_{yy}+\sigma^B_{\sigma\sigma}$. The transverse conductivity differs slightly from the transverse Lindhard conductivity we presented in Ref. [51], since the contribution of the spin term alters the result in the corner where q is large and ω small. This difference may be of importance if one considers near-field optics at surfaces, where an expansion in q can be relevant for a given frequency ω (see, e.g., Ref. [54]). The two small insets (g) and (h) show the results at the vacuum wave number $q=q_0$ for (g) the individual parts of the linear conductivity, and (h) the two independent elements of the total linear conductivity. No special features are present for $q=q_0$ in Fig. 5.

Independently of the fact that we have shown that the spin response in a part of the ω-q space is dominating the total linear conductivity (and the diamagnetic part is dominating the rest, except for some destructive interference with the paramagnetic part for small ω and large q), knowledge of the linear optical properties is important when we consider the screened nonlinear optical response later in our treatment (namely in Sec. IV).

2. Nonlinear conductivity

In Figs. 6 and 7 we have plotted the nonlinear nonlocal optical conductivity tensors, and as in the linear optical case they are plotted on a logarithmic scale as functions of the two independent variables q (normalized to k_F, as before) and $\hbar\omega$.

In the nonlinear optical response, two different diamagnetic processes contribute to the response, given by Eqs. (70) and (73). Figure 6(a) shows the modulus of one of them [the

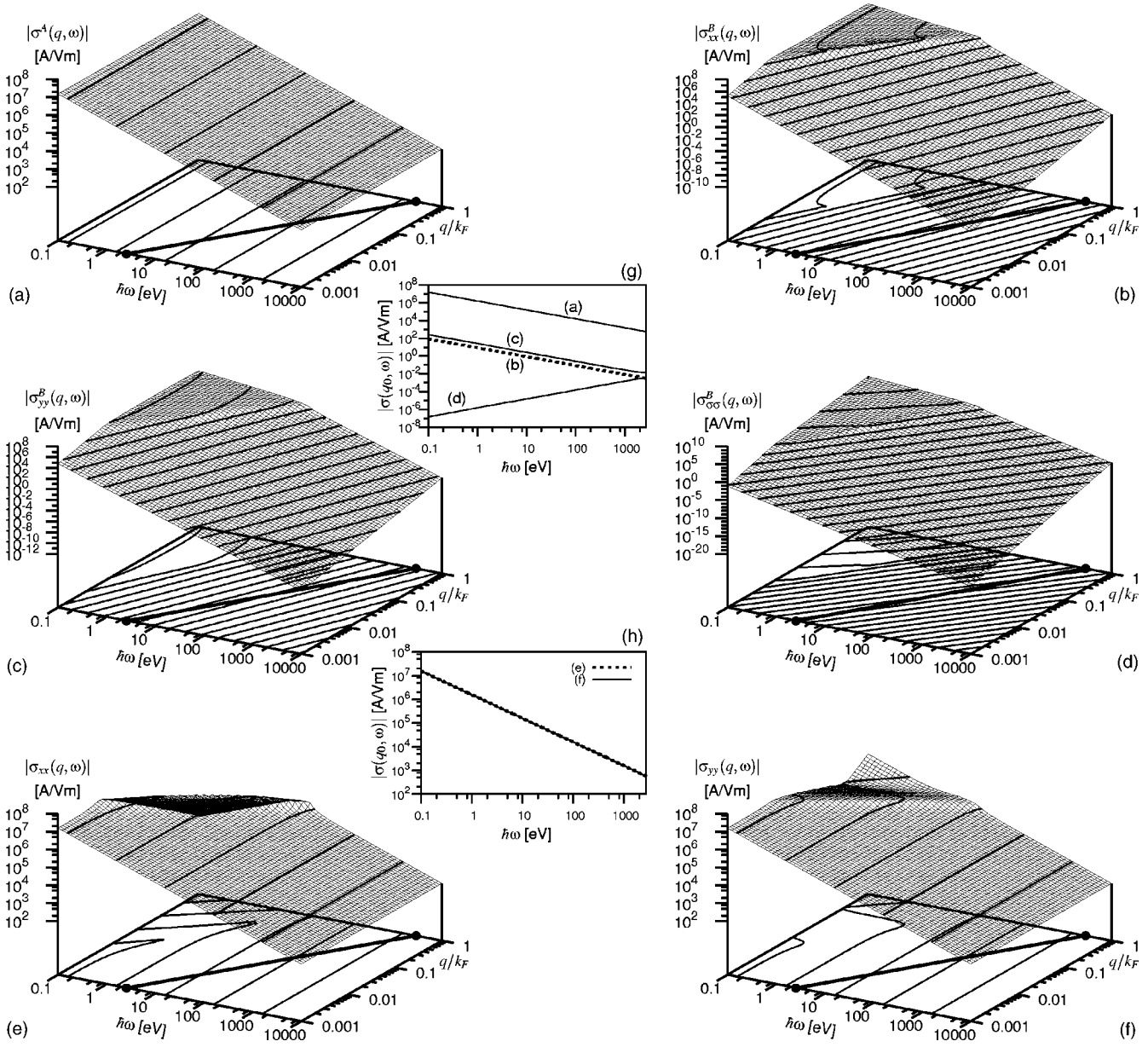

FIG. 5. Moduli of the linear conductivity tensor elements plotted as a function of the photon energy $\hbar\omega$ and the wave number normalized to the Fermi wavenumber (q/k_F). (a) is the diamagnetic linear conductivity $|\sigma^A|$, (b) the longitudinal paramagnetic conductivity $|\sigma^B_{xx}|$, (c) the transverse paramagnetic conductivity $|\sigma^B_{yy}|$, and (d) the spin conductivity $|\sigma^B_{\sigma\sigma}|$. The total linear conductivity tensor (compare to Fig. 3) element $|\sigma_{xx}|=|\sigma^A+\sigma^B_{xx}|$ is depicted in (e), and $|\sigma_{yy}|=|\sigma^A+\sigma^B_{yy}+\sigma^B_{\sigma\sigma}|$ in (f). Contours are plotted at every integer order of magnitude, and at the bottom of these plots is drawn a line at the vacuum wave number q_0. The insets show the results at $q=q_0$, where (g) shows the individual elements [as given in (a)–(d)] and (h) the total *xx* and *yy* elements [(e) and (f)]. (g) and (h) are cut off to the right at $q_0=k_F$ ($\hbar\omega=2.68$ keV).

one given by Eq. (70)], $|\Sigma^A|$. The other diamagnetic process, $|\Sigma^C_{xxx}|=2|\Sigma^C_{yxy}|$, is depicted in Fig. 6(f). The paramagnetic response described by Eq. (71) has, as determined in the symmetry analysis in Fig. 4, two independent nonzero elements, and $|\Sigma^B_{xxx}|$ is plotted in Fig. 6(b), while $|\Sigma^B_{xyy}|$ appears in Fig. 6(c). The spin conductivity $|\Sigma^B_{\sigma\sigma}|$ has two different nonzero elements, but since the difference is only a sign, the modulus remains the same. It is given by Eq. (73) and plotted in Fig. 6(d).

Looking at the orders of magnitude between the paramagnetic and spin conductivities, we observe that in most of the ω-q plane, the paramagnetic response prevails. However, at high photon energies and high q, the spin conductivity becomes more important. This is illustrated in Fig. 6(e), where the two contributions to the *xyy* element of the nonlinear conductivity have been added. In the high end of the spectrum there is an additional minimum (zero) where the magnitude of the two contributions become equal. In contrast to this stands the *yxy* element, where the addition of the spin contribution changes the amplitude of the response only, and none of the appearing features in Fig. 6(c) are changed qualitatively [thus the relevant plot is essentially the same plot as

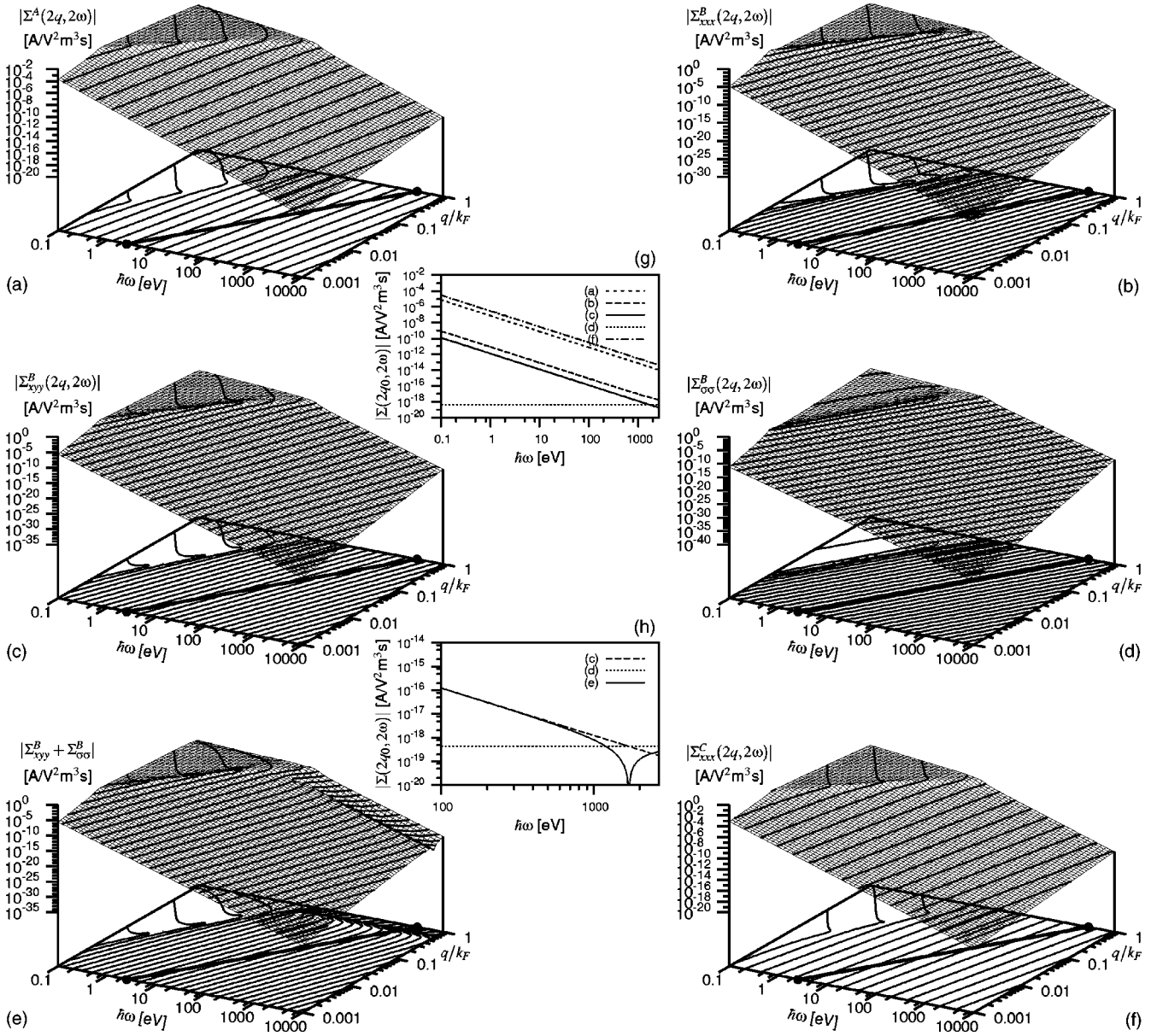

FIG. 6. Moduli of the nonlinear conductivity tensor elements are plotted as a function of the incoming photon energy $\hbar\omega$ and the wave number q normalized to the Fermi wave number k_F. (a) is the diamagnetic conductivity $|\Sigma^A|$, (b) the paramagnetic conductivity tensor element $|\Sigma^B_{xxx}|$, (c) the paramagnetic conductivity tensor element $|\Sigma^B_{xyy}|$, (d) the spin conductivity $|\Sigma^B_{\sigma\sigma}|$, (e) the sum of the paramagnetic and spin conductivities $|\Sigma^B_{xyy}+\Sigma^B_{\sigma\sigma}|$, and (f) the diamagnetic conductivity $|\Sigma^C_{xxx}|$. Contours are plotted at every integer order of magnitude, and at the bottom of each plot is drawn a line at the vacuum wave number q_0. The insets (g) and (h) show results at $q=q_0$, (g) for the individual elements of the conductivity tensor [compare (a)–(d) and (f)], and (h) for the paramagnetic *xyy* element, the spin element, and the sum of the two [compare (c)–(e)] in the region where a comparison is of interest. (g) and (h) are cut off to the right at $q_0=k_F$, as before (parts of this figure first appeared in Ref. [51]).

Fig. 6(c)]. Apart from this influence from the spin, if we look at the diamagnetic contribution in Fig. 6(f), we also expect this to give a significant contribution to the total nonlinear optical conducitivity in elements where it is present (and thus not to the *xyy* element). As in the linear case, we have shown the results at $q=q_0$ in the two small insets (g) and (h).

In order to get sufficient accuracy at the edges of the nonlinear conductivities, most notoriously at high photon energies and low values of q (roughly in the area of the lower right corner larger than $10q_0$) we had to go beyond the numerical precision given by the IEEE 754 standard [55]. We have done so by making use of Smith's multiple-precision FORTRAN90 routines FMLIB1.2 [56], and sufficient computer precision was reached with a 60-digit mantissa.

To complete the picture of the nonlinear optical conductivity tensor, we have in Fig. 7 plotted the moduli of the three resulting independent nonzero tensor elements when all contributions are added. Figure 7(a) shows the modulus of $|\Sigma_{xxx}|$, which is responsible for the coupling of the longitudinally polarized incoming field to a longitudinally polarized

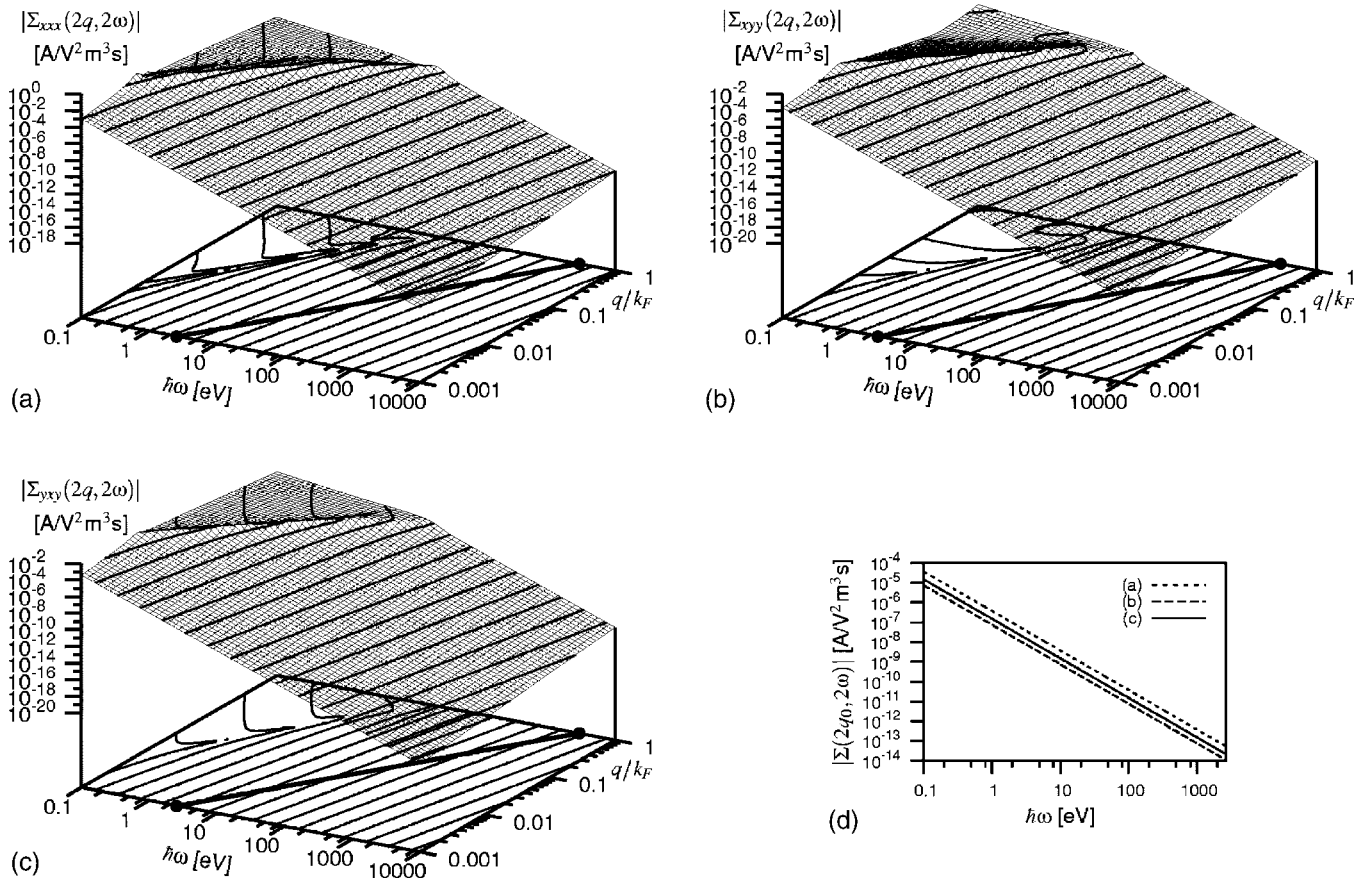

FIG. 7. Moduli of the three independent nonzero elements of the total nonlinear conductivity (compare Fig. 4 to see which elements contribute) tensor. (a) shows the tensor element $|\Sigma_{xxx}|$, (b) the tensor element $|\Sigma_{xyy}|$, and (c) the tensor element $|\Sigma_{yxy}|$. Contours are plotted at every integer order of magnitude, and at the bottom of each plot is drawn a line at the vacuum wave number q_0. (d) shows the results in (a)–(c) for $q=q_0$, cut off in the high end at $q_0=k_F$, as before.

second-harmonic field. A glance at Fig. 4 tells us that it consists of the paramagnetic and the diamagnetic terms, but is without contribution from the spin term. We observe that the influence of the diamagnetic response is dramatic, effectively enhancing the feature around $0.01q_0$ in the spectrum. In Fig. 7(b), the magnitude of the tensor element responsible for the coupling from a pure transversely polarized input field to a pure longitudinally polarized second-harmonic field is plotted, i.e., $|\Sigma_{xyy}|$. This tensor element has contributions from only one of the diamagnetic terms, but also from both the paramagnetic and the spin terms, as one recognizes from Fig. 4. Comparing to Fig. 6(e) we observe that the additional inclusion of the diamagnetic contribution removes the minimum that was present in the high end of the photon energy scale, but introduces changes to the part of the figure with low ω and high q. Figure 7(c) shows the last of the three nonzero tensor elements, $|\Sigma_{yxy}|$. It is responsible for the coupling of an input field with mixed longitudinal and transverse polarization to a second-harmonic field with transverse polarization. Here, Fig. 4 tells us that the other diamagnetic term contributes to the response in addition to the paramagnetic conductivity and the spin conductivity. Furthermore, the spin contribution has changed sign compared to the *xyy* element.

IV. RESPONSE TO A TRANSVERSE EXTERNAL ELECTROMAGNETIC FIELD

A. Local-field loop: General system

From the outset we assume that the parametric approximation can be adopted, i.e., we assume that the generated second-harmonic field does not affect the dynamics of the incident field. This approximation can be regarded as good, except for extremely high intensities or short time scales.

Before combining Eqs. (19) and (20) we convert Eq. (19) into an integral equation, namely

$$\boldsymbol{E}_{\mathrm{NL}}(\boldsymbol{r};2\omega) = \boldsymbol{E}^{\mathrm{ext}}(\boldsymbol{r};2\omega) - i2\mu_0\omega \int \overleftrightarrow{G}_0(\boldsymbol{r}-\boldsymbol{r}';2\omega)\cdot \boldsymbol{J}_{\mathrm{L}}(\boldsymbol{r}';2\omega)d^3r', \tag{74}$$

where $\boldsymbol{E}^{\mathrm{ext}}(\boldsymbol{r};2\omega)$ is the so-called external (ext) field driving the second-harmonic process, and $\overleftrightarrow{G}_0(\boldsymbol{r}-\boldsymbol{r}';2\omega)$ is the electromagnetic vacuum propagator taken at 2ω. A discussion of the electromagnetic vacuum propagator can be found in, e.g., Ref. [41], including how it is treated at the space point $\boldsymbol{r}-\boldsymbol{r}'=\boldsymbol{0}$ [we give the explicit form of $\overleftrightarrow{G}_0(\boldsymbol{r}-\boldsymbol{r}';2\omega)$ for three-

dimensional translationally invariant systems in Eq. (85)]. The last term of Eq. (74) accounts for the linear propagation of the generated field $\boldsymbol{E}_{\mathrm{NL}}(\boldsymbol{r};2\omega)$ through the nonlinear medium [$\boldsymbol{J}_{\mathrm{L}}(\boldsymbol{r}';2\omega)$ depends on $\boldsymbol{E}_{\mathrm{NL}}(\boldsymbol{r};2\omega)$, and thus Eq. (74) is self-consistent]. From a knowledge of the nonlinear part, $\boldsymbol{J}_{\mathrm{NL}}(\boldsymbol{r};2\omega)$, of the current density of the active medium, the external field can be calculated from the integral relation

$$\boldsymbol{E}^{\mathrm{ext}}(\boldsymbol{r};2\omega) = -i2\mu_0\omega \int \overleftrightarrow{G}_0(\boldsymbol{r}-\boldsymbol{r}';2\omega)\cdot\boldsymbol{J}_{\mathrm{NL}}(\boldsymbol{r}';2\omega)d^3r'. \tag{75}$$

In the parametric approximation adopted here the external field can be considered as a prescribed quantity. By inserting the linear constitutive equation [Eq. (20)] into Eq. (74) one obtains the following integral equation for the second-harmonic field:

$$\begin{aligned}\boldsymbol{E}_{\mathrm{NL}}(\boldsymbol{r};2\omega) &= \boldsymbol{E}^{\mathrm{ext}}(\boldsymbol{r};2\omega) - i2\mu_0\omega \\ &\times \int\int \overleftrightarrow{G}_0(\boldsymbol{r}-\boldsymbol{r}'';2\omega)\cdot\overleftrightarrow{\sigma}(\boldsymbol{r}'',\boldsymbol{r}';2\omega)\cdot\boldsymbol{E}_{\mathrm{NL}}(\boldsymbol{r}';2\omega) \\ &\times d^3r''d^3r'.\end{aligned} \tag{76}$$

The formal solution of this equation is given by

$$\boldsymbol{E}_{\mathrm{NL}}(\boldsymbol{r};2\omega) = \int \overleftrightarrow{\Gamma}(\boldsymbol{r},\boldsymbol{r}';2\omega)\cdot\boldsymbol{E}^{\mathrm{ext}}(\boldsymbol{r}';2\omega)d^3r', \tag{77}$$

where the nonlocal field-field response tensor $\overleftrightarrow{\Gamma}(\boldsymbol{r},\boldsymbol{r}';2\omega)$ is to be derived from the dyadic integral equation

$$\overleftrightarrow{\Gamma}(\boldsymbol{r},\boldsymbol{r}';2\omega) = \overleftrightarrow{\mathbb{1}}\delta(\boldsymbol{r}-\boldsymbol{r}') + \int \overleftrightarrow{K}(\boldsymbol{r},\boldsymbol{r}'';2\omega)\cdot\overleftrightarrow{\Gamma}(\boldsymbol{r}'',\boldsymbol{r}';2\omega)d^3r''. \tag{78}$$

In Eq. (78) the tensor

$$\overleftrightarrow{K}(\boldsymbol{r},\boldsymbol{r}'';2\omega) = -i2\mu_0\omega \int \overleftrightarrow{G}_0(\boldsymbol{r}-\boldsymbol{r}';2\omega)\cdot\overleftrightarrow{\sigma}(\boldsymbol{r}',\boldsymbol{r}'';2\omega)d^3r' \tag{79}$$

is the kernel of the integral equation (76). This kernel is formally identical to the one playing a prominent role in the electrodynamics of mesoscopic media and small particles [41].

By insertion of Eq. (75) into Eq. (77) and thereafter making use of Eq. (21), the second-harmonic field may in principle be calculated from known quantities. To solve the local-field loop for the linear response, one simply replaces NL with L and 2ω with ω in Eqs. (74)–(79) above.

In cases where the local field deviates only slightly from the external field the combination of Eqs. (19) and (20) is solved iteratively. In the first Born approximation, often employed in macroscopic electrodynamics the solution is

$$\begin{aligned}\boldsymbol{E}^{(1)}_{\mathrm{NL}}(\boldsymbol{r};2\omega) &= \boldsymbol{E}^{\mathrm{ext}}(\boldsymbol{r}';2\omega) - i2\mu_0\omega \\ &\times \int \overleftrightarrow{G}_0(\boldsymbol{r}-\boldsymbol{r}';2\omega)\cdot\overleftrightarrow{\sigma}(\boldsymbol{r}',\boldsymbol{r}'';2\omega)\cdot\boldsymbol{E}^{\mathrm{ext}}(\boldsymbol{r}'';2\omega) \\ &\times d^3r''d^3r',\end{aligned} \tag{80}$$

the second Born approximation gives

$$\begin{aligned}\boldsymbol{E}^{(2)}_{\mathrm{NL}}(\boldsymbol{r};2\omega) &= \boldsymbol{E}^{\mathrm{ext}}(\boldsymbol{r}';2\omega) - i2\mu_0\omega \\ &\times \int \overleftrightarrow{G}_0(\boldsymbol{r}-\boldsymbol{r}';2\omega)\cdot\overleftrightarrow{\sigma}(\boldsymbol{r}',\boldsymbol{r}'';2\omega)\cdot\boldsymbol{E}^{(1)}_{\mathrm{NL}}(\boldsymbol{r}'';2\omega) \\ &\times d^3r''d^3r',\end{aligned} \tag{81}$$

and so on, and so forth.

If one wishes to go beyond the above-mentioned series of Born approximations, a procedure one can apply in order to achieve a numerical solution to Eq. (76) is the so-called "coupled antenna theory," in which the separability of the spatial coordinates in $\overleftrightarrow{\sigma}(\boldsymbol{r},\boldsymbol{r}')$ is in focus. This separability makes it possible to rewrite the integral equation problem as a matrix problem involving the energy eigenstates of the electronic system. For details, we refer interested readers to Ref. [41].

B. Local-field loop: Homogeneous system

If one wishes to do an experimental observation of these phenomena, it is necessary also to consider the influence of the electronic screening. The convolution integral [Eq. (79)] has the Fourier-space representation

$$\boldsymbol{E}_{\mathrm{L}}(\boldsymbol{q},\omega) = \boldsymbol{E}^{\mathrm{ext}}_{\mathrm{L}}(\boldsymbol{q},\omega) - i\mu_0\omega\overleftrightarrow{G}_0(\boldsymbol{q},\omega)\cdot\overleftrightarrow{\sigma}(\boldsymbol{q},\omega)\cdot\boldsymbol{E}_{\mathrm{L}}(\boldsymbol{q},\omega), \tag{82}$$

$$\begin{aligned}\boldsymbol{E}_{\mathrm{NL}}(2\boldsymbol{q},2\omega) &= \boldsymbol{E}^{\mathrm{ext}}_{\mathrm{NL}}(2\boldsymbol{q},2\omega) \\ &- i2\mu_0\omega\overleftrightarrow{G}_0(2\boldsymbol{q},2\omega)\cdot\overleftrightarrow{\sigma}(2\boldsymbol{q},2\omega)\cdot\boldsymbol{E}_{\mathrm{NL}}(2\boldsymbol{q},2\omega),\end{aligned} \tag{83}$$

where $\boldsymbol{E}^{\mathrm{ext}}_{\mathrm{L}}(\boldsymbol{q},\omega)$ is the external (laser) field, and

$$\boldsymbol{E}^{\mathrm{ext}}_{\mathrm{NL}}(2\boldsymbol{q},2\omega) = -i2\mu_0\omega\overleftrightarrow{G}_0(2\boldsymbol{q},2\omega)\cdot\boldsymbol{J}_{\mathrm{NL}}(2\boldsymbol{q},2\omega). \tag{84}$$

The electromagnetic propagator contains both a transverse and a longitudinal part, and its Fourier amplitude can be written [see Ref. [57], Eq. (50)] as a sum of a transverse propagator and a longitudinal self-field propagator,

$$\overleftrightarrow{G}_0(\boldsymbol{q},\omega) = \frac{\overleftrightarrow{\mathbb{1}} - \boldsymbol{e}_{\boldsymbol{q}}\otimes\boldsymbol{e}_{\boldsymbol{q}}}{q_0^2-q^2} + \frac{\boldsymbol{e}_{\boldsymbol{q}}\otimes\boldsymbol{e}_{\boldsymbol{q}}}{q_0^2}, \tag{85}$$

where $q_0=\omega/c_0$ is the free-space wave vector. In a homogeneous electron gas with $\boldsymbol{q}\|\boldsymbol{e}_x$, it becomes

$$\overleftrightarrow{G}_0(\boldsymbol{q},\omega) = \frac{1}{q_0^2 - q^2}\left[\overleftrightarrow{\mathbb{I}} - \frac{q^2}{q_0^2}\boldsymbol{e}_x \otimes \boldsymbol{e}_x\right]. \tag{86}$$

Since both $\overleftrightarrow{G}_0$ and $\overleftrightarrow{\sigma}$ are diagonal here, the self-consistent solution to the electrodynamics is reduced to an algebraic one, namely

$$E_{\mathrm{L},i}(\boldsymbol{q},\omega) = \frac{E^{\mathrm{ext}}_{\mathrm{L},i}(\boldsymbol{q},\omega)}{1 + i\mu_0\omega G_{0,ii}(\boldsymbol{q},\omega)\sigma_{ii}(\boldsymbol{q},\omega)}, \tag{87}$$

$$E_{\mathrm{NL},i}(2\boldsymbol{q},2\omega) = \frac{E^{\mathrm{ext}}_{\mathrm{NL},i}(2\boldsymbol{q},2\omega)}{1 + i2\mu_0\omega G_{0,ii}(2\boldsymbol{q},2\omega)\sigma_{ii}(2\boldsymbol{q},2\omega)}, \tag{88}$$

$\forall i \in \{x,y,z\}$. Expressing also the latter one in terms of the laser field, we find by insertion of Eq. (84)

$$\begin{aligned} E_{\mathrm{NL},i}(2\boldsymbol{q},2\omega) = \frac{1}{(2\pi)^3}\sum_{jk} & \frac{-2i\mu_0\omega G_{0,ii}(2\boldsymbol{q},2\omega)\Sigma_{ijk}(2\boldsymbol{q},2\omega)}{1 + 2i\mu_0\omega G_{0,ii}(2\boldsymbol{q},2\omega)\sigma_{ii}(2\boldsymbol{q},2\omega)} \\ & \times \frac{E^{\mathrm{ext}}_{\mathrm{L},j}(\boldsymbol{q},\omega)}{1 + i\mu_0\omega G_{0,jj}(\boldsymbol{q},\omega)\sigma_{jj}(\boldsymbol{q},\omega)} \\ & \times \frac{E^{\mathrm{ext}}_{\mathrm{L},k}(\boldsymbol{q},\omega)}{1 + i\mu_0\omega G_{0,kk}(\boldsymbol{q},\omega)\sigma_{kk}(\boldsymbol{q},\omega)}. \end{aligned} \tag{89}$$

The screened linear and nonlinear optical conductivities can then be found by comparing the current densities $\boldsymbol{J}^{\mathrm{scr}}_{\mathrm{L}}(\boldsymbol{q},\omega) = \overleftrightarrow{\sigma}(2\boldsymbol{q},2\omega)\cdot\boldsymbol{E}_{\mathrm{L}}(\boldsymbol{q},\omega)$ and $\boldsymbol{J}^{\mathrm{scr}}_{\mathrm{NL}}(2\boldsymbol{q},2\omega) = \overleftrightarrow{\sigma}(2q,2\omega)\cdot\boldsymbol{E}_{\mathrm{NL}}(\boldsymbol{q},\omega)$, respectively, to the need of expressing these quantities in terms of the laser field $[\boldsymbol{E}^{\mathrm{ext}}_{\mathrm{L}}(\boldsymbol{q},\omega)]$ rather than the self-consistent fields. Thus the current generated at the detector in terms of the laser field is written

$$\boldsymbol{J}^{\mathrm{scr}}_{\mathrm{L}}(\boldsymbol{q},\omega) \equiv \overleftrightarrow{\xi}(\boldsymbol{q},\omega)\cdot\boldsymbol{E}^{\mathrm{ext}}_{\mathrm{L}}(\boldsymbol{q},\omega), \tag{90}$$

$$\boldsymbol{J}^{\mathrm{scr}}_{\mathrm{NL}}(2\boldsymbol{q},2\omega) \equiv \frac{1}{(2\pi)^3}\overleftrightarrow{\Xi}(2\boldsymbol{q},2\omega):\boldsymbol{E}^{\mathrm{ext}}_{\mathrm{L}}(\boldsymbol{q},\omega)\boldsymbol{E}^{\mathrm{ext}}_{\mathrm{L}}(\boldsymbol{q},\omega), \tag{91}$$

where we have defined screened linear ($\overleftrightarrow{\xi}$) and nonlinear ($\overleftrightarrow{\Xi}$) nonlocal conductivity tensors in terms of the nonscreened ones, i.e.,

$$\xi_{ii}(\boldsymbol{q},\omega) = \frac{\sigma_{ii}(\boldsymbol{q},\omega)}{1 + i\mu_0\omega G_{0,ii}(\boldsymbol{q},\omega)\sigma_{ii}(\boldsymbol{q},\omega)}, \tag{92}$$

$$\begin{aligned} \Xi_{ijk}(2\boldsymbol{q},2\omega) = & -\frac{2i\mu_0\omega\sigma_{ii}(2\boldsymbol{q},2\omega)G_{0,ii}(2\boldsymbol{q},2\omega)\Sigma_{ijk}(2\boldsymbol{q},2\omega)}{1 - 2i\mu_0\omega G_{0,ii}(2\boldsymbol{q},2\omega)\sigma_{ii}(2\boldsymbol{q},2\omega)} \\ & \times \frac{1}{1 + i\mu_0\omega G_{0,jj}(\boldsymbol{q},\omega)\sigma_{jj}(\boldsymbol{q},\omega)} \\ & \times \frac{1}{1 + i\mu_0\omega G_{0,kk}(\boldsymbol{q},\omega)\sigma_{kk}(\boldsymbol{q},\omega)}. \end{aligned} \tag{93}$$

It is important here to underscore the fact that the above-mentioned screened linear and nonlinear optical conductivity tensors fulfil the Kramers-Kronig relations and the Einstein causality, while the unscreened ones in general do not.

The relevant observable is the intensity of the outcoming electromagnetic fields. It is calculated as

$$I(\boldsymbol{q},\omega) = \frac{\varepsilon_0 c_0}{2}\frac{\boldsymbol{E}(\boldsymbol{q},\omega)\cdot\boldsymbol{E}^*(\boldsymbol{q},\omega)}{(2\pi)^6} \approx 2.16\times 10^{-8}|\boldsymbol{E}(\boldsymbol{q},\omega)|^2, \tag{94}$$

where the factor of $(2\pi)^{-6}$ arises from the way we have defined the electric field.

1. Linear response

As with the direct conductivities, let us consider the linear optical response first. Thus, in Fig. 8, moduli of the screened linear optical conductivities are plotted as functions of the photon energy and the normalized wave number q/k_F. Figures 8(a) and 8(c) show the full screened linear tensor elements, $|\xi_{xx}|$ and $|\xi_{yy}|$, respectively, i.e., all terms are included both above and below the division line in Eq. (92). In all other plots, whenever a term is neglected, it is neglected both above and below this division line. To see the influence of the different nonparamagnetic terms on the normally assumed dominating paramagnetic contribution, we have in Fig. 8(b) plotted $|\xi_{xx}|$ taking into account only the paramagnetic contribution. Similarly, in Fig. 8(d), the spin contribution to $|\xi_{yy}|$ is neglected, in Fig. 8(e) the diamagnetic contribution to $|\xi_{yy}|$ is neglected, and in Fig. 8(f), both the spin and the diamagnetic contributions to $|\xi_{yy}|$ are neglected. We observe that also in the screened linear conductivity the spin contributes to the response in the region where ω is small and q is large [compare Figs. 8(c) and 8(d)]. The diamagnetic contribution is again the dominating one. Additionally, we notice the presence of resonances, which we shall discuss at the end of this section.

In order to emphasize the behavior at $q=q_0$ (at a group velocity of c_0) [58], we have in Figs. 8(g) and 8(h) plotted the results of Figs. 8(a)–8(f) at $q=q_0$. Figure 8(g) also reveals the bottom of the resonance observed in (c), and especially $|\xi_{yy}|$ appears quite different in the general overview plot in ω-q space than at $q=q_0$. This is a very deep and narrow creek in ω-q space, and impossible to show to its full extent in a general overview. $|\xi_{xx}|$, on the other hand, reveals no additional information at $q=q_0$. To access the rest ($q \neq q_0$) of the ω-q space, one in general has to resort to using so-called *evanescent waves*. In Fig. 8(h) we observe the effect on $|\xi_{yy}|$, should one neglect the spin term, the diamagnetic term, or both, when considering only q_0. It shows that at $q=q_0$, only the energy range above around 500 eV reveals the difference, and thus one might be led to conclude that the influence of spin and diamagnetism is very small. This is in contrast to the conclusion one can draw from the overview figures, where (i) it is visible that the spin contributes in the region of low photon energies and high values of q [(c) vs (d)], (ii) there are collective resonances present (see Sec. IV B 3 below), and (iii) the magnitude is in most of the ω-q space much larger when spin and diamagnetism are included. Hence, if evanescent waves are used, diamagnetic (and at low frequencies also the spin) contributions should not be neglected.

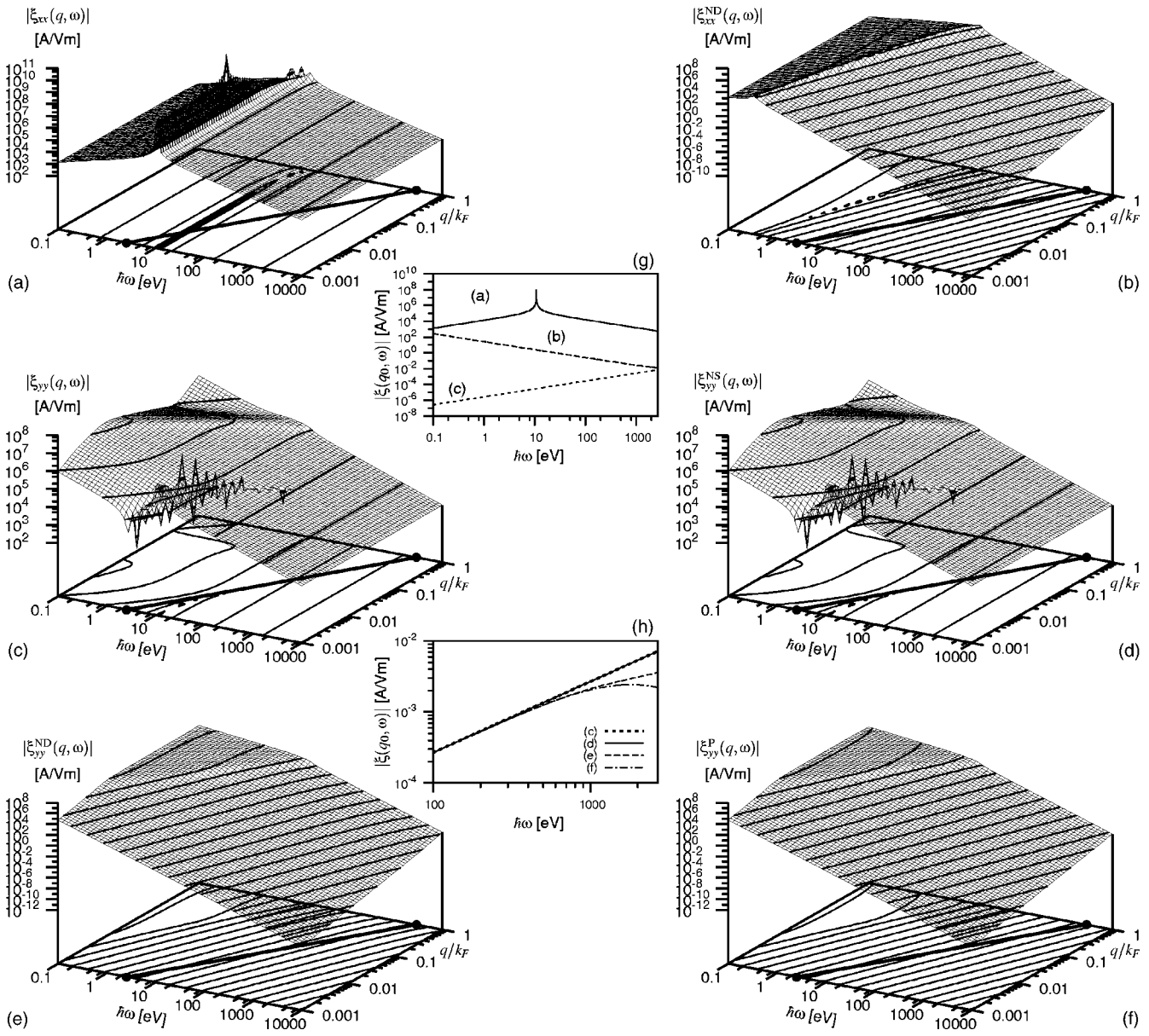

FIG. 8. Moduli of the screened linear conductivity. In (a), it is $|\xi_{xx}|$ with all terms included, while in (b) the diamagnetic term is neglected. In (c), it is $|\xi_{yy}|$ with all terms included, while in (d) the spin term is neglected, in (e) the diamagnetic term is neglected, and in (f) both the spin and diamagnetic terms are neglected. Contours are plotted at every integer order of magnitude, and at the bottom of each plot is drawn a line at the vacuum wave number q_0. The insets (g) and (h) show the results for $q=q_0$, corresponding to the plots (a)–(c) and (c)–(f), respectively.

2. Nonlinear response

Having presented the screened linear conductivity we can go on with the nonlinear one, described by Eq. (93). We notice that in Eq. (93), the screened nonlinear optical response contains linear responses at the fundamental and the second-harmonic frequencies in the screening term. Thus the linear optical properties have an influence on the nonlinear optical properties in this way.

In Fig. 9 we have plotted the moduli of the screened nonlinear nonlocal conductivity tensor elements, with the complete tensor elements in the left column and the corresponding ones for the pure paramagnetic (P) response (i.e., all diamagnetic and spin terms are neglected, also in the screening) in the right column. The upper row shows these two cases for $|\Xi_{xxx}|$, the middle row for $|\Xi_{xyy}|$, and the lower row for $|\Xi_{yxy}|$. As in the linear case, we have emphasized the result at $q=q_0$, showing in Fig. 9(g) the full tensor elements, and in Fig. 9(h) the paramagnetic (P) contributions. We observe that screening has an influence on all three tensor elements, although for those leading to a longitudinal response ($|\Xi_{xxx}|$ and $|\Xi_{xyy}|$) it is not as dramatic as in the one leading to a transverse response, i.e., in $|\Xi_{yxy}|$. Additionally, we observe that neglecting the spin and the diamagnetic parts leads to significant changes in the slopes (rate of falloff with large ω for constant q, i.e., denser contours), although at $q=q_0$ the

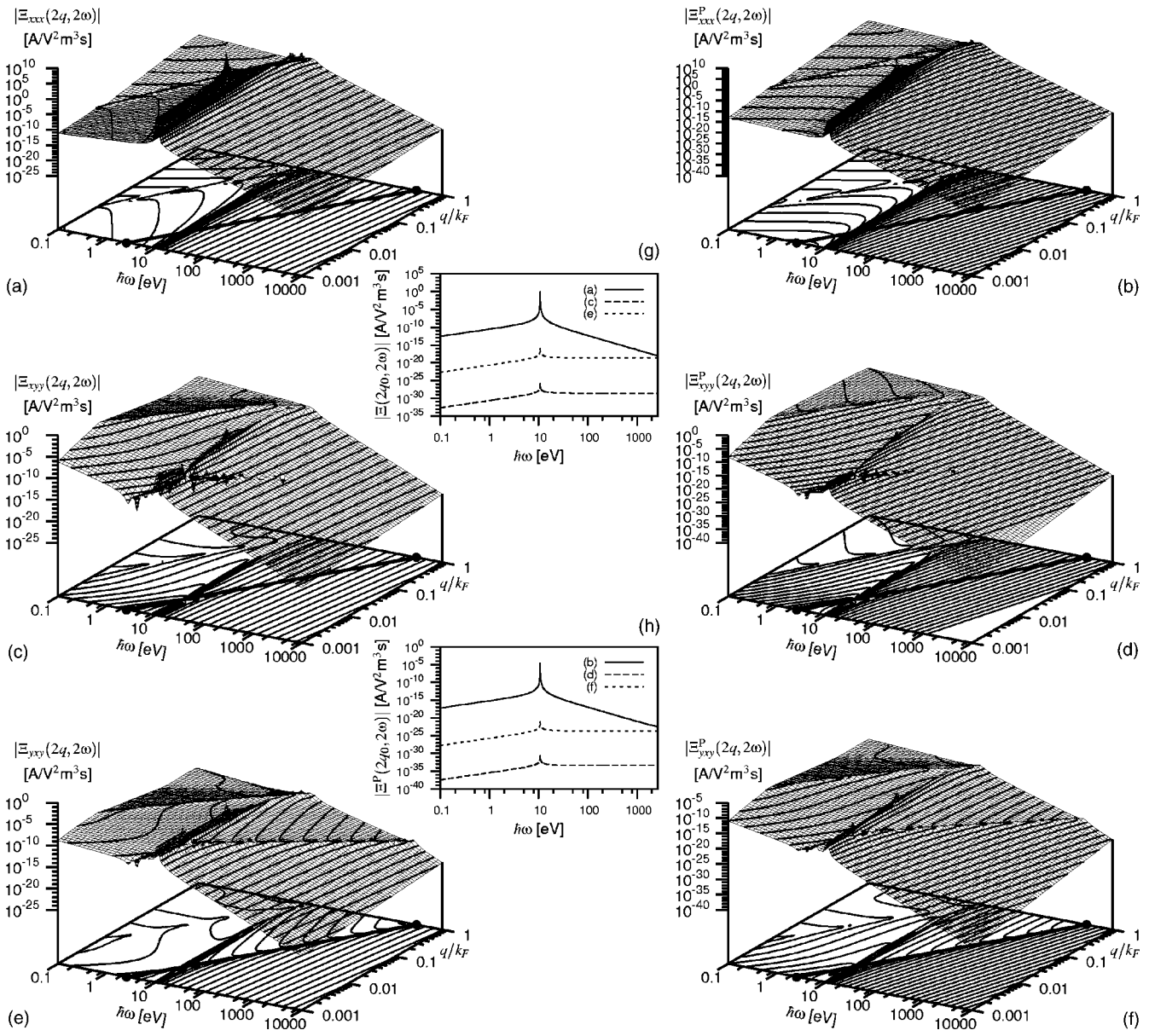

FIG. 9. Moduli of the screened nonlinear conductivity. The leftmost column shows the full tensor elements, and the rightmost column the tensor elements arising if only the paramagnetic response is considered. In (a) is a plot of $|\Xi_{xxx}|$ with all terms included, and the same element with only the paramagnetic contribution is shown as (b). In (c) is shown $|\Xi_{xyy}|$ with all terms included, and the corresponding pure paramagnetic result is given in (d). Finally, (e) represents $|\Xi_{yxy}|$ with all terms included, and (f) the corresponding pure paramagnetic result. Contours are plotted at every integer order of magnitude, and at the bottom of each plot is drawn a line at the vacuum wave number q_0. The insets show the results for $q=q_0$, in (g) for the full screened nonlocal conductivity tensor elements, and in (h) if only the paramagnetic contributions are included.

only difference appears to be in the order of magnitude of the results.

The effect of neglecting either diamagnetism or spin, in stead of none or both of them, is illustrated in Fig. 10. $|\Xi_{xxx}|$ does not contain contributions from the spin, so neglecting the diamagnetic term is equal to just considering the paramagnetic response, as shown in Fig. 9(b). Figure 10(a) shows the modulus of $|\Xi_{xyy}|$ when spin is included and diamagnetism is neglected (ND), while in Fig. 10(b), it is opposite (NS). Similarly, Fig. 10(c) contains the modulus of $|\Xi_{yxy}|$ when spin is included and diamagnetism is neglected, and Fig. 10(d) shows the case where it is opposite. At $q=q_0$, the results are as shown in Fig. 10(e). Comparing Fig. 10 with Fig. 9, it is evident that neglecting any of the spin or diamagnetic contributions produces qualitatively different results than including all of them.

Now that all individual screened nonlinear conductivity tensor elements have been addressed, it is time to look at the different possible optical configurations. The incoming light can be polarized either longitudinally (parallel to $\boldsymbol{q}$, here along the x axis) or transversely (perpendicular to $\boldsymbol{q}$, in the y-z plane). A pure longitudinal input results in a pure longitu-

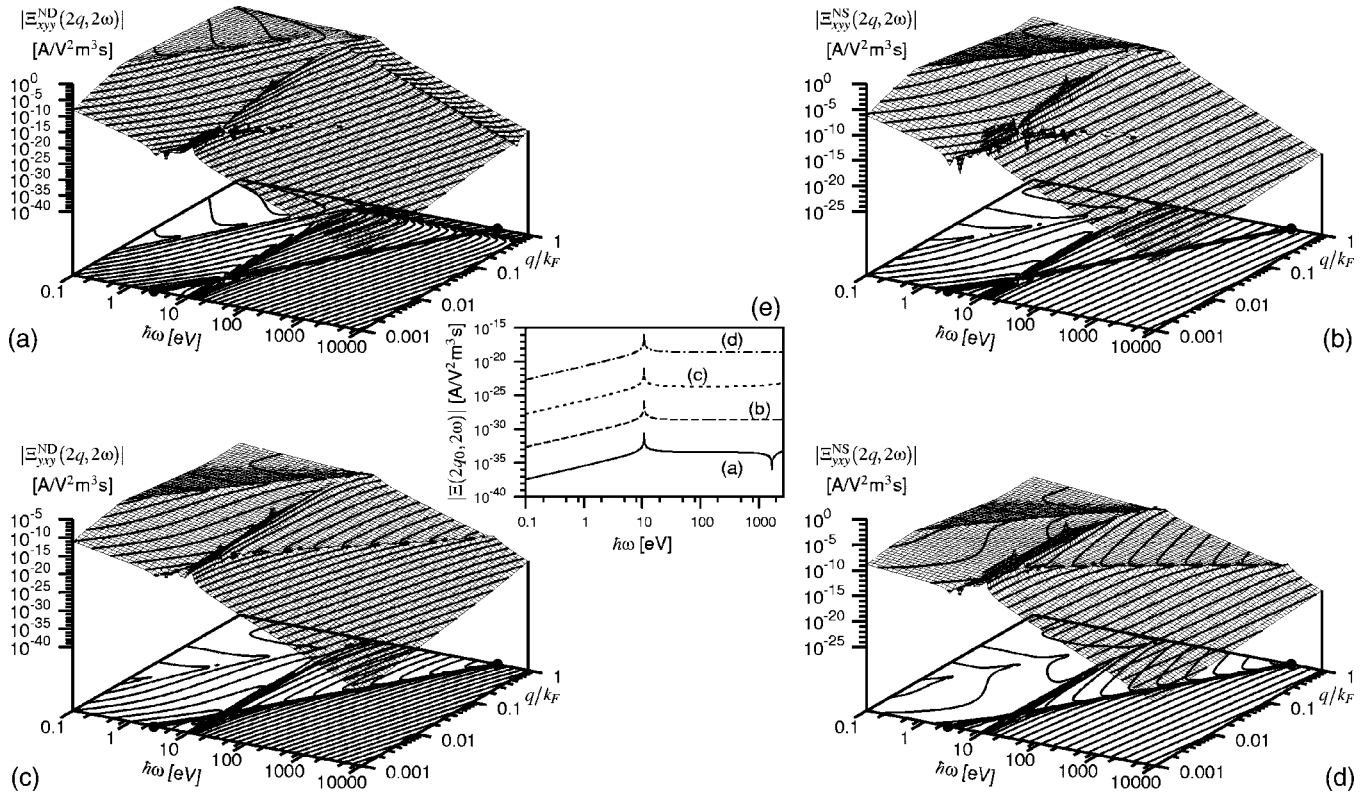

FIG. 10. Moduli of the screened nonlinear conductivity (compare Fig. 9). The leftmost column shows tensor elements when diamagnetism is neglected and spin is included, and the rightmost column shows the tensor elements when the spin contribution is neglected and diamagnetism is included. (a) and (b) for $|\Xi_{xyy}|$, while (c) and (d) are for $|\Xi_{yxy}|$. Contours are plotted at every integer order of magnitude, and at the bottom of each plot is drawn a line at the vacuum wave number q_0. The inset (e) shows the results for $q=q_0$.

dinal output, and the corresponding result can be directly derived from Fig. 9(a). Similarly, a pure transverse input also results in a pure longitudinal second-harmonic output, which is directly proportional to Fig. 9(c). Thus two of the screened nonlinear optical conductivity tensors are directly available in an experimental setup, while the remaining one is not. To probe the influence of Ξ_{yxy}, one has to mix longitudinal and transverse polarization in the input. In the presence of a polarizer to select the transverse output polarization, this is directly proportional to the result shown in Fig. 9(e), whereas if such a selection is not present, one gets the combined response of $|\Xi_{xxx}+\Xi_{xyy}+2\Xi_{yxy}|$ (assuming that the two polarizations have the same strength, and that the transverse polarization is along the y axis), as shown in Fig. 11. Comparing Figs. 11 and 9 we observe that the sum is essentially a sum of the magnitudes of the three terms, with no new features arising from a destructive interference between any of the terms.

3. Collective resonances

In the screened linear and nonlinear conductivities, collective resonances are present where the denominators in Eqs. (92) and (93) become zero, i.e., when

$$1 + i\mu_0\omega G_{0,xx}(q,\omega)\sigma_{\mathrm{L}}(q,\omega) = 1 + \frac{i\sigma_{xx}(q,\omega)}{\varepsilon_0\omega} = 0, \quad (95)$$

in longitudinal screening (nonretarded, called a *plasmon* resonance), and when

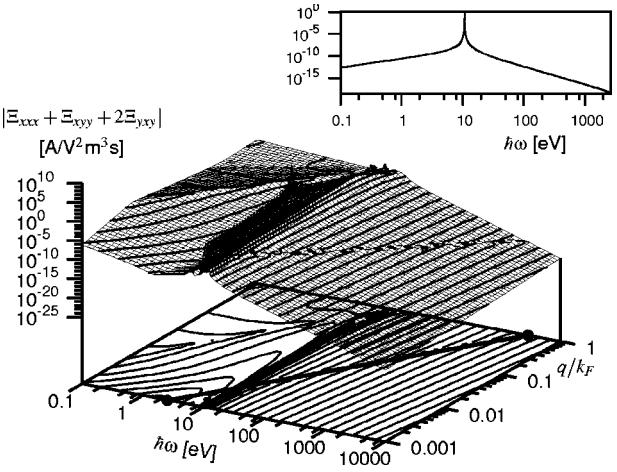

FIG. 11. Modulus of the screened nonlinear conductivity for mixed longitudinal and transverse input polarization and likewise mixed output polarization, $|\Xi_{xxx}+\Xi_{xyy}+2\Xi_{yxy}|$. Contours are plotted at every integer order of magnitude, and at the bottom of each plot is drawn a line at the vacuum wave number q_0. The inset shows the result at $q=q_0$.

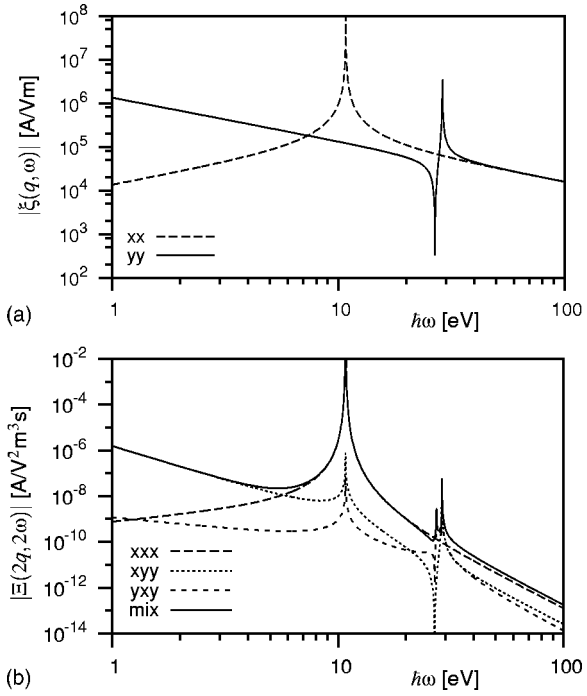

FIG. 12. Collective resonances are present in the form of plasmons and plasmaritons in the screened (a) linear and (b) nonlinear responses. Results are shown for $q=0.01k_F$. The legend refers to the individual tensor elements, except "mix," which refers to Fig. 11.

$$1 + i\mu_0\omega G_{0,yy}(q,\omega)\sigma_{yy}(q,\omega) = 1 + \frac{i\sigma_{yy}(q,\omega)}{[1-(q/q_0)^2]\varepsilon_0\omega} = 0, \tag{96}$$

in transverse screening (retarded by c_0, called a *plasmariton* resonance). One should notice that while the longitudinal screening factor equals the *xx* component of the relative dielectric tensor, the transverse screening factor *does not* equal the *yy* component of this tensor (see Ref. [51]).

Looking at Figs. 8–11, several collective resonances are present. The *plasmon* resonance is varying only slightly with the value of q, and appears almost constant just above 10 eV in Figs. 8–11. The *plasmariton* resonances have the same asymptotic energy for $q\to 0$ as the plasmon, while for large values of q, their position in ω-q space approaches the line of $q=\omega/c_0$ asymptotically.

In order to emphasize the effect of the collective resonances, we have in Fig. 12 plotted the screened linear (a) and nonlinear (b) conductivities in the relevant energy range for $q=0.01k_F$. In Fig. 12(a) $\xi_{xx}(q,\omega)$ (dashed line) features a plasmon resonance just above 10 eV, while in $\xi_{yy}(q,\omega)$ (solid line) a plasmariton resonance is present a little to the right of the minimum that occurs at $q=q_0$. In the nonlinear conductivities, shown in Fig. 12(b), the plasmon resonance is again present just above 10 eV. There are two different plasmariton resonances present. One appears with double degeneracy in $\Xi_{xyy}(2q,2\omega)$, since it originates in the screening of the laser field. The other one appears as one out of two nondegenerate plasmariton resonances in $\Xi_{yxy}(2q,2\omega)$. It originates in the second-harmonic field. The "mixed" conductivity contains all three resonances, as one would expect.

V. USING DFT WITH OUR MODEL

It is already well known that in order to describe the second-harmonic response of centrosymmetric media [59] one has to go away from the local electric-dipole approximation. In the present paper, we have shown that inclusion of the spin and diamagnetic terms influence the nonlinear optical response, even in a simple model for the bulk response such as the homogeneous electron gas. We should mention that the importance of diamagnetism has previously been stressed for lower-dimensional systems [60,61].

In practical applications of solid-state physics, one of course has to replace the free-electron gas with, e.g., a bulk periodic potential and, eventually, include spin-orbit and exchange interactions, as well as correlation effects, at which point not only *all* of the processes of Figs. 1 and 2 will be present (nonzero), but additional processes will arise explicitly. That it is technically feasible to perform calculations of nonlinear optics from real solid-state systems is indicated in, e.g., Ref. [62], where the nonlinear optical response of an Fe monolayer on Cu has been studied using the full-potential linearized augmented plane-wave (LAPW) [63] method in the electric-dipole approximation. The additional burden of including nonlocality in the response should not prevent any calculation, as we shall indicate in the discussion below.

In the perspective of *ab initio* calculations with reduced basis sets, such as the LAPW method, the present results for the homogeneous electron gas can be seen as a first-order approximation to the so-called *interstitial* region (LAPW and other reduced-basis-set methods usually divide space into so-called *muffin tins* around each atom, inside which an atom-alone-in-the-world approach is taken, and an interstitial region comprising everything outside the muffin tins). In order to complete a treatment relevant for use with LAPW (or any other bulk *ab initio* method), one would have to rewrite the theory in terms of this basis set, i.e., in LAPW, spherical harmonics inside the muffin tins and plane waves with the inclusion of Bloch functions (for the periodic lattice) in the interstitial region, and thus also allow for the different weighting factors of the wave functions that appear. Therefore one would have to (i) go back to the real-space expressions given in Eqs. (42)–(44) for the linear optical properties, Eqs. (47)–(50) for the nonlinear optical properties, and Eqs. (74)–(79) for the treatment of electronic screening effects [alternatively, Eq. (80) if one wishes to use the shortcut that the Born approximation provides]; (ii) insert the desired basis set(s) and Bloch functions according to the symmetry present in crystals under consideration; and (iii) transform these new expressions into $\boldsymbol{k}$ space as needed.

With the present state of the art [64], and the evolution in computing power and storage for technical computing, we believe that calculations of nonlocal optical properties using *ab inito* methods are becoming feasible, at least in the region where the crystal lattice is stable. A possible strategy to perform such calculations for real metals involves five steps, namely (i) to determine the ground state (which computer codes based on density-functional theory are generally good at) and converge the $\boldsymbol{k}$ mesh and crystal potential to an accuracy that is sufficient to generate well-converged optical properties at $\boldsymbol{q}=\boldsymbol{0}$ [62]; (ii) to introduce additional $\boldsymbol{k}$ points at

$\boldsymbol{k}+\boldsymbol{q}$, $\boldsymbol{k}+2\boldsymbol{q}$, etc., as required in the formulas; (iii) to recalculate the ground state with this new set of $\boldsymbol{k}$ points in order to produce the corresponding eigenstates, (iv) to calculate the nonlocal optical responses along the ω axis using this set of eigenstates, (v) to change the value of $\boldsymbol{q}$ and repeat the procedure from point (ii) as needed. This can all be done with a single self-consistent solution to the crystal potential, obtained in step (i), and the added computing time varies linearly with the desired number of $\boldsymbol{q}$ steps, without resorting to second variational methods such as $\boldsymbol{k}\cdot\boldsymbol{p}$. With careful selection of the $\boldsymbol{q}$ points, the calculation time can be further reduced.

If one wants to use real-space *ab initio* codes in order to calculate the second-harmonic response of clusters or molecules, the analytic part of the work becomes a lot easier, since one can start directly with Eqs. (42)–(44), Eqs. (47)–(50), and Eqs. (74)–(79), once the eigenfunctions and eigenenergies have been determined.

VI. SUMMARY OF CONCLUSIONS

To conclude, we have presented a theory for calculating the linear and nonlinear optical properties from the Pauli Hamiltonian. Special emphasis has been given to the simple homogeneous electron gas, and numerical results based on the developed theory have proven that diamagnetism, spin, and screening are all important ingredients in describing linear and nonlinear optics more accurately than the common paramagnetism-only approach. Finally, we have discussed the relation of our theory to existing numerical methods in condensed-matter theory, and we have proposed a way of performing *ab initio* calculations that scale linearly (or better) with the number of $\boldsymbol{q}$ points.

Seeing such interesting effects of the spin already in the three-dimensional electron gas is certainly an indication that further effects of the influence of the spin on nonlinear optics may be revealed if one considers low-dimentional systems such as the two-dimensional electron gas (quantum well) or the one-dimensional quantum wire. It is furthermore expected that these features will be present also in more realistic models of solid-state systems.

ACKNOWLEDGMENTS

T.A. would like to acknowledge financial support from the European Union research training networks DYNASPIN (Contract No. ERB-FMRX-CT97-0124), EXCITING (Contract No. HPRN-CT-2002-00317), as well as from the German Science Foundation research program SFB418.

APPENDIX A: CURRENT DENSITIES AND TRANSITION MATRIX ELEMENTS

The microscopic current-density is given by [65,66]

$$\boldsymbol{j}(\boldsymbol{r},t)=\boldsymbol{j}_F(\boldsymbol{r})+\boldsymbol{j}_F^{\sigma}(\boldsymbol{r})+\frac{1}{2}[\boldsymbol{j}_1(\boldsymbol{r};\omega)e^{-i\omega t}+\text{c.c.}], \tag{A1}$$

where

$$\boldsymbol{j}_F(\boldsymbol{r})=-\frac{e}{2m_e}[\boldsymbol{p}\,\delta(\boldsymbol{r}-\boldsymbol{r}_e)+\delta(\boldsymbol{r}-\boldsymbol{r}_e)\boldsymbol{p}], \tag{A2}$$

$$\boldsymbol{j}_F^{\sigma}(\boldsymbol{r})=\frac{ie}{2m_e}[\boldsymbol{p}\,\delta(\boldsymbol{r}-\boldsymbol{r}_e)-\delta(\boldsymbol{r}-\boldsymbol{r}_e)\boldsymbol{p}]\times\boldsymbol{\sigma} \tag{A3}$$

are the spin-independent and spin-dependent contributions to the free (F) current density, respectively, $\boldsymbol{r}_e$ is the position of the electron, $\boldsymbol{p}$ operates on the $\boldsymbol{r}_e$ space, and

$$\boldsymbol{j}_1(\boldsymbol{r};\omega)=-\frac{e^2}{m_e}\boldsymbol{A}(\boldsymbol{r}_e;\omega)\,\delta(\boldsymbol{r}-\boldsymbol{r}_e) \tag{A4}$$

is the vector-potential dependent current density, which together with the second-order interaction Hamiltonian ensures that we get a gauge invariant result for the single-electron response.

With the spinor wave functions of Eq. (31), the transition matrix elements for the current densities become

$$\langle n,s|\boldsymbol{j}_F(\boldsymbol{r})|n',s'\rangle=-\frac{e\hbar}{2im_e}(\psi_n^*\boldsymbol{\nabla}\psi_{n'}-\psi_{n'}\boldsymbol{\nabla}\psi_n^*)\,\delta_{ss'}, \tag{A5}$$

$$\begin{aligned}\langle n,s|\boldsymbol{j}_F^{\sigma}(\boldsymbol{r})|n',s'\rangle&=-\frac{e\hbar}{2m_e}(\psi_n^*\boldsymbol{\nabla}\psi_{n'}+\psi_{n'}\boldsymbol{\nabla}\psi_n^*)\times\langle s|\boldsymbol{\sigma}|s'\rangle\\&\equiv\langle n|\boldsymbol{j}_F^{s}(\boldsymbol{r})|n'\rangle\times\langle s|\boldsymbol{\sigma}|s'\rangle,\end{aligned} \tag{A6}$$

and

$$\langle n,s|\boldsymbol{j}_1(\boldsymbol{r};\omega)|n',s'\rangle=-\frac{e^2}{m_e}\langle n|\,\delta(\boldsymbol{r}-\boldsymbol{r}_e)|n'\rangle\delta_{ss'}\boldsymbol{A}(\boldsymbol{r};\omega). \tag{A7}$$

Above, we have defined a new quantity, $\langle n|\boldsymbol{j}_F^{s}(\boldsymbol{r})|n'\rangle$, in order to separate the spin and space contributions.

The matrix elements of the different terms in the interaction Hamiltonian thus become

$$\langle n,s|\mathcal{H}_1(\boldsymbol{r};\omega)|n',s'\rangle=-\int\langle n|\boldsymbol{j}_F(\boldsymbol{r})|n'\rangle\delta_{ss'}\cdot\boldsymbol{A}(\boldsymbol{r};\omega)d^3r, \tag{A8}$$

$$\begin{aligned}\langle n,s|\mathcal{H}_1^{\sigma}(\boldsymbol{r};\omega)|n',s'\rangle&=-\int\langle n,s|\boldsymbol{j}_F^{\sigma}(\boldsymbol{r})|n',s'\rangle\cdot\boldsymbol{A}(\boldsymbol{r};\omega)d^3r\\&=-\int\langle n|\boldsymbol{j}_F^{s}(\boldsymbol{r})|n'\rangle\\&\quad\times\langle s|\boldsymbol{\sigma}|s'\rangle\cdot\boldsymbol{A}(\boldsymbol{r};\omega)d^3r.\end{aligned} \tag{A9}$$

With two spin states, say $s_1=\binom{1}{0}$ and $s_2=\binom{0}{1}$, there are four combinations of $\langle s|\boldsymbol{\sigma}|s'\rangle$, namely $\langle s_1|\boldsymbol{\sigma}|s_1\rangle=\boldsymbol{e}_z$, $\langle s_1|\boldsymbol{\sigma}|s_2\rangle=\sqrt{2}\boldsymbol{e}_-$, $\langle s_2|\boldsymbol{\sigma}|s_1\rangle=\sqrt{2}\boldsymbol{e}_+$, and $\langle s_2|\boldsymbol{\sigma}|s_2\rangle=-\boldsymbol{e}_z$, where $\boldsymbol{e}_\pm=(\boldsymbol{e}_x\pm i\boldsymbol{e}_y)/\sqrt{2}$.

APPENDIX B: INTEGRALS IN THE 3-D ELECTRON GAS

Below, we discuss the analytic solution to the integrals over $\boldsymbol{k}$ appearing in the linear [Eqs. (62)–(64)] and nonlinear

TABLE II. Identification of the orders p, v, r, and β of the generalized type of integrals [Eq. (B1)] appearing in the different parts of the linear and nonlinear conductivity tensors. The comma between numbers in p indicates the different values it can take. v, r, and β, on the other hand, are unique for each element. In the Cartesian coordinate system, $k_y=k_z=k_\perp$ when $k_x=k_\parallel \| q$. Thus v and r are interchangeable.

Tensor	Element	Order-deciding part	p	v	r	β
$\vec{\sigma}^B$	xx	$4k_\parallel^2+4k_\parallel q+q^2$	0,1,2	0	0	1
	$yy=zz$	$4k_\perp^2$	0	0	2	1
$\vec{\sigma}^B_{\sigma\sigma}$	$yy=zz$	1	0	0	0	1
$\vec{\Sigma}^A$	$xxx=xyy=xzz$	$k_\parallel+q$	0,1	0	0	1
$\vec{\Sigma}^B$	xxx	$4k_\parallel^3-k_\parallel q^2$	1,3	0	0	2
	$xyy=xzz=yxy=zxz=yyx=zzx$	$4k_\parallel k_\perp^2$	1	0	2	2
$\vec{\Sigma}^B_{\sigma\sigma}$	$xyy=xzz$	$-k_\parallel$	1	0	0	2
	$yxy=yyx=zxz=zzx$	$k_\parallel$	1	0	0	2
$\vec{\Sigma}^C$	xxx	$4k_\parallel+2q$	0,1	0	0	1
	$yyx=yxy=zzx=zxz$	$2k_\parallel+q$	0,1	0	0	1

[Eqs. (70)–(73)] conductivity tensors in the low-temperature limit. Every integral over $\boldsymbol{k}$ in both the linear and the nonlinear conductivity tensor can, when $\boldsymbol{q}\|\boldsymbol{e}_x$, be expressed as a sum over terms of the general type

$$\mathfrak{F}^\beta_{pvr}(\{a\},\{b\},s)=\int\int\int \frac{k_x^p k_y^v k_z^r f(\boldsymbol{k}+s\boldsymbol{e}_x)}{\prod_{j=1}^\beta [a_j k_x+b_j]}dk_x dk_y dk_z, \tag{B1}$$

where p,v,r,j,β are nonnegative integers, and the integration runs over the whole $\boldsymbol{k}$ space. The functions in general depend on (i) a set of real quantities, $\{a\}\equiv\{a_1,\ldots,a_\beta\}$ appearing in front of the integration variable k_x in the denominator, (ii) a set of complex nonzero quantities, $\{b\}\equiv\{b_1,\ldots,b_\beta\}$ appearing as the other quantity in each term of the denominator, and (iii) the real quantity s representing the displacement of the center of the Fermi-Dirac distribution function sphere from $(k_x,k_y,k_z)=(0,0,0)$. The quantity s together with each element in the set $\{a\}$ is in general a function of the wave vectors, $\boldsymbol{q}$ and $\boldsymbol{k}$. Each element in the set $\{b\}$ is furthermore a function of τ, the relaxation time.

One observes that in Eq. (B1) a cylindrical symmetry is present in the Cartesian coordinate system, because the two directions y and z are equivalent in a 3DEG where $\boldsymbol{q}\|\boldsymbol{e}_x$. However, in the low-temperature limit the Fermi-Dirac distribution function is zero outside the Fermi sphere and equal to one inside, and it is therefore advantageous to shift k_x by $-s$, followed by a one-to-one mapping of the Cartesian coordinate system into *spherical* coordinates (ρ-ϕ-θ). Although the above-mentioned cylindrical symmetry is thereby removed in the expressions, it should obviously appear again after integration. This property can thus be used to check the results. Using in this way $k_x=\rho\sin\phi\cos\theta$, $k_y=\rho\sin\phi\sin\theta$, and $k_z=\rho\cos\phi$, we calculate the Jacobian determinant for this mapping, and thus $dk_x dk_y dk_z=\rho^2\sin\phi d\rho d\phi d\theta$. Thereby the indefinite integral in Eq. (B1) is turned into the definite integral

$$\mathfrak{F}^\beta_{pvr}(\{a\},\{b\},s)=\int_0^{k_F}\int_0^{\pi}\int_0^{2\pi}\frac{\rho^2\sin\phi(\rho\sin\phi\cos\theta-s)^p}{\prod_{j=1}^\beta[a_j(\rho\sin\phi\cos\theta-s)+b_j]}\times(\rho\sin\phi\sin\theta)^v(\rho\cos\phi)^r d\theta d\phi d\rho. \tag{B2}$$

Looking at the relevant equations for the conductivity tensors, we observe that $\vec{\sigma}^A$ has no denominator. The properties of the others are summarized in Table II. It reflects the consequences of the cylindrical symmetry in the Cartesian coordinate system. Therefore, integrals with indices $(v,r)=(0,2)$ gives the same results as for indices $(v,r)=(2,0)$, and we may choose to drop one of them, say v, by setting $v=0$ and defining $\mathfrak{F}^\beta_{pr}\equiv\mathfrak{F}^\beta_{p0r}$. A further reduction in the complexity of the total solution is possible, since functions with $\beta=2$ can be expressed in terms of functions with $\beta=1$ in the following way:

$$\mathfrak{F}^2_{pr}(a_1,a_2,b_1,b_2,s)=\frac{a_1\mathfrak{F}^1_{pr}(a_1,b_1,s)-a_2\mathfrak{F}^1_{pr}(a_2,b_2,s)}{a_1b_2-a_2b_1}, \tag{B3}$$

$a_j\neq 0, j\in\{1,2\}$. If any a_j, say, a_1, is zero, we observe from Eq. (B2) that the order (in k_x) of the denominator is decreased by one, and thus, that $\mathfrak{F}^2_{pr}(0,a_2,b_1,b_2,s)=\mathfrak{F}^1_{pr}(a_2,b_2,s)/b_1$.

As a consequence of the interchangeability of the indices v and r, and of Eq. (B3), the integrals appearing can now be written in terms of functions of the type

$$\mathfrak{F}^1_{pr}(a,b,s)=\int_0^{k_F}\int_0^{\pi}\int_0^{2\pi}\frac{\rho^2\sin\phi(\rho\sin\phi\cos\theta-s)^p}{b-as+a\rho\sin\phi\cos\theta}\times(\rho\cos\phi)^r d\theta d\phi d\rho, \tag{B4}$$

dropping the now superfluous index on a and b. Before solving Eq. (B4) in the cases needed, let us mention that in the special case where $a=0$ (i.e., when $q=0$), the solution is

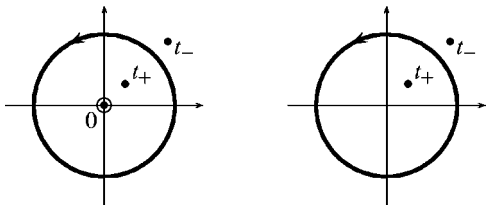

FIG. 13. The poles in the complex t-plane in Eq. (B8) are of order 1 at $t_\pm$ and of order h at $t=0$, as shown to the left. To the right is shown the case where $h=0$ and the pole at $t=0$ vanishes. The closed contour shown in each diagram is the integration path used.

trivial, and can be left as an exercise to the reader. Thus, after carrying out the integrals, two specific tests can be applied in order to verify the results, namely (i) letting $a\to 0$ in the final expressions, and (ii) showing that an explicit calculation of $(v,r)=(2,0)$ in Eq. (B2) gives the results of $\mathfrak{F}^1_{02}(a,b,s)$ and $\mathfrak{F}^1_{12}(a,b,s)$.

When $a\neq 0$, we have to consider the full solution to Eq. (B4) for the different combinations of p, $v=0$, and r mentioned in Table II. To solve Eq. (B4), let us make the substitutions $\eta\equiv(b-as)/(ak_F)$, $\rho\equiv k_F u$, giving $d\rho=k_F du$, and

$$\frac{d\rho}{b-as+a\rho\,\sin\,\phi\,\cos\,\theta}=\frac{1}{a}\frac{du}{\eta+u\,\sin\,\phi\,\cos\,\theta}. \quad \text{(B5)}$$

Thereby we get

$$\mathfrak{F}^1_{pr}=\frac{k_F^{2+r}}{a}\int_0^1\int_0^\pi\int_0^{2\pi}\frac{u^{2+r}(k_F u\,\sin\,\phi\,\cos\,\theta-s)^p}{\eta+u\,\sin\,\phi\,\cos\,\theta}\times\sin\,\phi\,\cos^r\phi\,d\theta\,d\phi\,du, \quad \text{(B6)}$$

where for brevity we have left out the reference to a, b, s in $\mathfrak{F}^1_{pr}$, since all $\mathfrak{F}^1_{pr}$ are functions of exactly one of each of them from here.

First, we look at the integrals over θ. Having Table II in mind, we observe that the numerator varies as $\cos^h\theta$, with $h\in\{0,1,2,3\}$ and contains only even orders of $\sin\,\theta$, which can be expressed in terms of $\cos\,\theta$ by use of $\sin^2\theta+\cos^2\theta=1$ [integrals with odd powers of $\sin\,\theta$ in Eq. (B4) would vanish anyway if they were present]. Letting $w=u\,\sin\,\phi$, we thus need to solve the integral

$$\int_0^{2\pi}\frac{\cos^h\theta}{\eta+w\,\cos\,\theta}d\theta,\quad \forall\, h\in\{0,1,2,3\}. \quad \text{(B7)}$$

Using a contour integration along the unit circle, i.e., letting $t=\exp(i\theta)$, we get $\cos\,\theta=(t^2+1)/(2t)$ and $dt/d\theta=i\,\exp(i\theta)=it$. Thereby the integral becomes

$$\int_0^{2\pi}\frac{\cos^h\,\theta}{\eta+w\,\cos\,\theta}d\theta=\frac{2}{2^h iw}\oint_{|t|=1}\frac{(t^2+1)^h}{t^h(t-t_+)(t-t_-)}dt, \quad \text{(B8)}$$

with poles at $t_\pm=-(\eta/w)\pm\sqrt{(\eta/w)^2-1}$, and for $h>0$ also at $t=0$. As illustrated in Fig. 13, one pole is outside the unit circle, and the other two are inside. Using the unit circle as the integration path, a residue calculation gives [67]

$$\int_0^{2\pi}\frac{\cos^h\theta}{\eta+w\,\cos\,\theta}d\theta=\frac{\pi}{w}\Theta(h-3)+\frac{2\pi}{w}\Theta(h-1)\left(-\frac{\eta}{w}\right)^{h-1}+\left(-\frac{\eta}{w}\right)^h\frac{2\pi}{\sqrt{\eta^2-w^2}}, \quad \text{(B9)}$$

$\forall h\in\{0,1,2,3\}$, and where $\Theta(x)=0$ for $x<0$ and $\Theta(x)=1$ for $x\geqslant 0$. Insertion into the relevant $\mathfrak{F}^1_{pr}$ functions gives

$$\mathfrak{F}^1_{00}=\frac{2\pi k_F^2}{a}\int_0^1 u^2\int_0^\pi\frac{\sin\,\phi}{\sqrt{\eta^2-u^2\sin^2\phi}}d\phi\,du, \quad \text{(B10)}$$

$$\mathfrak{F}^1_{02}=\frac{2\pi k_F^4}{a}\int_0^1 u^4\int_0^\pi\frac{\sin\,\phi-\sin^3\phi}{\sqrt{\eta^2-u^2\sin^2\phi}}d\phi\,du, \quad \text{(B11)}$$

$$\mathfrak{F}^1_{10}=\frac{2\pi k_F^3}{a}\int_0^1 u^2\int_0^\pi\left[\sin\,\phi-\left(\eta+\frac{s}{k_F}\right)\frac{\sin\,\phi}{\sqrt{\eta^2-u^2\sin^2\phi}}\right]\times d\phi\,du, \quad \text{(B12)}$$

$$\mathfrak{F}^1_{12}=\frac{2\pi k_F^5}{a}\int_0^1 u^4\int_0^\pi\left[\sin\,\phi\,\cos^2\phi-\left(\eta+\frac{s}{k_F}\right)\frac{\sin\,\phi-\sin^3\phi}{\sqrt{\eta^2-u^2\sin^2\phi}}\right]d\phi\,du, \quad \text{(B13)}$$

$$\mathfrak{F}^1_{20}=\frac{2\pi k_F^4}{a}\int_0^1 u^2\int_0^\pi\left[\left(\eta^2+\frac{2s\eta}{k_F}+\frac{s^2}{k_F^2}\right)\frac{\sin\,\phi}{\sqrt{\eta^2-u^2\sin^2\phi}}-\left(\eta+\frac{2s}{k_F}\right)\sin\,\phi\right]d\phi\,du, \quad \text{(B14)}$$

$$\mathfrak{F}^1_{30}=\frac{2\pi k_F^5}{a}\int_0^1 u^2\int_0^\pi\left[\frac{u^2}{2}\sin^3\phi+\left(\frac{3s^2}{k_F^2}+\frac{3s\eta}{k_F}+\eta^2\right)\sin\,\phi-\left(\eta^3+\frac{3s\eta^2}{k_F}+\frac{3s^2\eta}{k_F^2}+\frac{s^3}{k_F^3}\right)\frac{\sin\,\phi}{\sqrt{\eta^2-u^2\sin^2\phi}}\right]d\phi\,du, \quad \text{(B15)}$$

and we are left with a number of trivial integrals, and the three nontrivial ones,

$$\int_0^\pi\int_0^1\frac{u^h\sin^k\phi}{\sqrt{\eta^2-u^2\sin^2\phi}}du\,d\phi, \quad \text{(B16)}$$

$\forall(h,k)\in\{(2,1),(4,1),(4,3)\}$.Using a binomial series expansion [68] of the square root, i.e.,

$$(1+x)^{-1/2}=\sum_{n=0}^\infty\frac{(-1)^n(2n-1)!!}{(2n)!!}x^n \quad \text{(B17)}$$

and the identity

$$\int_0^{\pi/2}\sin^{2m+1}x\,dx=\frac{(2m)!!}{(2m+1)!!}, \quad \text{(B18)}$$

we find, after a little algebra, the solutions

$$\int_0^{\pi}\int_0^{1}\frac{u^2\sin\phi}{\sqrt{\eta^2-u^2\sin^2\phi}}dud\phi=\sum_{n=0}^{\infty}\frac{2}{\eta^{2n+1}}\frac{1}{(2n+3)(2n+1)}=\frac{1}{2}\left[(1-\eta^2)\ln\frac{\eta+1}{\eta-1}+2\eta\right], \tag{B19}$$

$$\int_0^{\pi}\int_0^{1}\frac{u^4\sin\phi}{\sqrt{\eta^2-u^2\sin^2\phi}}dud\phi=\sum_{n=0}^{\infty}\frac{2}{\eta^{2n+1}}\frac{1}{(2n+5)(2n+1)}=\frac{1}{4}\left[(1-\eta^4)\ln\frac{\eta+1}{\eta-1}+\frac{2\eta}{3}+2\eta^3\right], \tag{B20}$$

$$\int_0^{\pi}\int_0^{1}\frac{u^4\sin^3\phi}{\sqrt{\eta^2-u^2\sin^2\phi}}dud\phi=\sum_{n=0}^{\infty}\frac{2}{\eta^{2n+1}}\frac{2n+2}{(2n+5)(2n+3)(2n+1)}=\frac{1}{8}\left[(1+2\eta^2-3\eta^4)\ln\frac{\eta+1}{\eta-1}+6\eta^3-2\eta\right]. \tag{B21}$$

Looking at the radius of convergence for the sums above, we can conclude that they are generally convergent in the regime where $q\leqslant k_F$, above which we anyway would be limited by the model. Since now all relevant integrals have been solved, we can present the analytic expressions for the relevant combinations of p, and r of Eq. (B1), as they are listed in Table II. They are

$$\mathfrak{F}_{00}^1=\frac{\pi k_F^2}{a}\left[(1-\eta^2)\ln\frac{\eta+1}{\eta-1}+2\eta\right], \tag{B22}$$

$$\mathfrak{F}_{02}^1=\frac{\pi k_F^4}{4a}\left[(1-\eta^2)^2\ln\frac{\eta+1}{\eta-1}+\frac{10\eta}{3}-2\eta^3\right], \tag{B23}$$

$$\mathfrak{F}_{10}^1=\frac{\pi k_F^3}{a}\left\{\frac{4}{3}-\frac{b}{ak_F}\left[(1-\eta^2)\ln\frac{\eta+1}{\eta-1}+2\eta\right]\right\}, \tag{B24}$$

$$\mathfrak{F}_{12}^1=\frac{\pi k_F^5}{a}\left\{\frac{4}{15}-\frac{1}{4}\frac{b}{ak_F}\left[(1-\eta^2)^2\ln\frac{\eta+1}{\eta-1}+\frac{10\eta}{3}-2\eta^3\right]\right\}, \tag{B25}$$

$$\mathfrak{F}_{20}^1=\frac{\pi k_F^4}{a}\left\{\left(\frac{b}{ak_F}\right)^2\left[(1-\eta^2)\ln\frac{\eta+1}{\eta-1}+2\eta\right]-\frac{4}{3}\left(\frac{b}{ak_F}+\frac{s}{k_F}\right)\right\}, \tag{B26}$$

$$\mathfrak{F}_{30}^1=\frac{\pi k_F^5}{a}\left\{\frac{4}{15}+\frac{4}{3}\left[\frac{b}{ak_F}\left(\frac{b}{ak_F}+\frac{s}{k_F}\right)+\frac{s^2}{k_F^2}\right]-\left(\frac{b}{ak_F}\right)^3\left[(1-\eta^2)\ln\frac{\eta+1}{\eta-1}+2\eta\right]\right\}. \tag{B27}$$

Finally, we apply the two previously mentioned tests. Calculation of the limit where $a=0$ can conveniently be done using a power series expansion of the logarithm involved, i.e.,

$$\frac{1}{2}\ln\frac{\eta+1}{\eta-1}=\sum_{n=0}^{\infty}\frac{1}{(2n+1)\eta^{2n+1}}. \tag{B28}$$

Substituting η with its original definition and subsequently letting $a=0$ in the resulting expressions, we obtain the same result as if we directly let $a=0$ in Eq. (B4). To further verify the solutions, explicit calculations have been carried out, and they show that, indeed, by interchanging v and r (as given in Table II) in Eq. (B2) we arrive at the same results as above. Q.E.D.

APPENDIX C: CONDUCTIVITY TENSORS INTEGRATED

Below, the linear and nonlinear conductivity tensors are expressed as functions of the general solutions presented in Appendix B, Eqs. (B22)–(B27).

The diamagnetic linear conductivity tensor [Eq. (62)], where $\beta=0$, has the solution

$$\sigma^A=\frac{ie^2k_F^3}{3\pi^2\omega m_e}. \tag{C1}$$

In the paramagnetic and the spin-dependent linear conductivity tensors, $\beta=1$, and we get, according to Table II,

$$\sigma_{xx}^B=\frac{ie^2\hbar}{16\pi^3m_e^2\omega}[4\,\mathfrak{F}_{20}^1(a,b_1,q)-4\,\mathfrak{F}_{20}^1(a,b_1,0)+4q\,\mathfrak{F}_{10}^1(a,b_1,q)-4q\,\mathfrak{F}_{10}^1(a,b_1,0)+q^2\,\mathfrak{F}_{00}^1(a,b_1,q)-q^2\,\mathfrak{F}_{00}^1(a,b_1,0)], \tag{C2}$$

$$\sigma_{yy}^B=\frac{ie^2\hbar}{4\pi^3m_e^2\omega}[\mathfrak{F}_{02}^1(a,b_1,q)-\mathfrak{F}_{02}^1(a,b_1,0)], \tag{C3}$$

$$\sigma_{\sigma\sigma}^B=\frac{ie^2\hbar q^2}{16\pi^3m_e^2\omega}[\mathfrak{F}_{00}^1(a,b_1,q)-\mathfrak{F}_{00}^1(a,b_1,0)], \tag{C4}$$

with $a=\hbar q/m_e$ and $b_1=\hbar q^2/(2m_e)-\omega-i/\tau$.

The only independent element of part A of the nonlinear conductivity thus becomes, again referring to Table II,

$$\Sigma^A=\frac{e^3}{32\pi^3m_e^2\omega^2}[\mathfrak{F}_{10}^1(2a,b_2,2q)-\mathfrak{F}_{10}^1(2a,b_2,0)+q\,\mathfrak{F}_{00}^1(2a,b_2,2q)-q\,\mathfrak{F}_{00}^1(2a,b_2,0)], \tag{C5}$$

with a as above and $b_2=2\hbar q^2/m_e-2\omega-i/\tau$. In the paramagnetic and the spin-dependent nonlinear conductivity tensors, $\beta=2$, and we thus get

$$\vec{\Sigma}^B = \frac{e^3\hbar}{64\pi^3 m_e^3\omega^2}[\vec{\Omega}(2a,a,b_3,b_1,q) - \vec{\Omega}(2a,a,b_3,b_1,0) - \vec{\Omega}(2a,a,b_3,b_4,0) + \vec{\Omega}(2a,a,b_3,b_4,-q)], \quad \text{(C6)}$$

$$\vec{\Sigma}^B_{\sigma\sigma} = \frac{e^3\hbar q^2}{32\pi^3 m_e^3\omega^2}[\vec{\Omega}^\sigma(2a,a,b_3,b_1,q) - \vec{\Omega}^\sigma(2a,a,b_3,b_1,0) - \vec{\Omega}^\sigma(2a,a,b_3,b_4,0) + \vec{\Omega}^\sigma(2a,a,b_3,b_4,-q)], \quad \text{(C7)}$$

with a as above, $b_3=-2\omega-i/\tau$, and $b_4=-\hbar q^2/(2m_e)-\omega-i/\tau$. The nonzero elements of the third rank tensors $\vec{\Omega}$ and $\vec{\Omega}^\sigma$ are defined using Table II as $\Omega_{xxx}=4\,\mathfrak{F}^2_{30}-q^2\mathfrak{F}^2_{10}$, $\Omega_{xyy}=4\,\mathfrak{F}^2_{12}$, $\Omega^\sigma_{xyy}=-\mathfrak{F}^2_{10}$, and $\Omega^\sigma_{yxy}=\mathfrak{F}^2_{10}$, in short notation, since the argument of the different Ω_{ijk} and Ω^σ_{ijk} applies to each of the $\mathfrak{F}^\beta_{pr}$-functions appearing.

Finally, the nonzero elements of part C of the nonlinear conductivity tensor are $\Sigma^C_{yyx}=\Sigma^C_{xxx}/2$, and

$$\Sigma^C_{xxx} = \frac{e^3}{16\pi^3 m_e^2\omega^2}[2\,\mathfrak{F}^1_{10}(a,b_1,q) - 2\,\mathfrak{F}^1_{10}(a,b_1,0) + q\,\mathfrak{F}^1_{00}(a,b_1,q) - q\,\mathfrak{F}^1_{00}(a,b_1,0)], \quad \text{(C8)}$$

with a and b_1 as defined above. In the sharp limit we get

$$\Sigma^A(2q,2\omega) = \frac{3ne^3uz}{8m_e\hbar\omega^2 q}\left\{1+\frac{1}{8z}\left[[1-(u-2z)^2]\ln\left|\frac{2z-u+1}{2z-u-1}\right| + [1-(u+2z)^2]\ln\left|\frac{2z+u+1}{2z+u-1}\right|\right]\right\}, \quad \text{(C9)}$$

$$\Sigma^B_{xxx}(2q;2\omega) = \frac{3ne^3}{64m_e\hbar\omega^2 q}\frac{u}{z^2}\left\{(u^2-z^2)\left[[1-(u-2z)^2]\ln\left|\frac{2z-u+1}{2z-u-1}\right| + [1-(u+2z)^2]\ln\left|\frac{2z+u+1}{2z+u-1}\right| + 8z\right]\right.$$
$$\left. - 2(u^2+2z^2)\left[[1-(u+z)^2]\ln\left|\frac{z+u+1}{z+u-1}\right| + [1-(u-z)^2]\ln\left|\frac{z-u+1}{z-u-1}\right| + 4z\right]\right\}, \quad \text{(C10)}$$

$$\Sigma^B_{xyy}(2q;2\omega) = \frac{3ne^3}{256m_e\hbar\omega^2 q}\frac{u}{z^2}\left\{[1-(u-2z)^2]^2\ln\left|\frac{2z-u+1}{2z-u-1}\right| + [1-(u+2z)^2]^2\ln\left|\frac{2z+u+1}{2z+u-1}\right| - 24z^3 - 2\left[[1-(u+z)^2]^2\ln\left|\frac{z+u+1}{z+u-1}\right| + [1-(u-z)^2]^2\ln\left|\frac{z-u+1}{z-u-1}\right|\right]\right\}, \quad \text{(C11)}$$

$$\Sigma^B_{\sigma\sigma,xyy}(2q;2\omega) = \frac{3ne^3u}{32m_e\hbar\omega^2 q}\left\{2\left[[1-(u+z)^2]\ln\left|\frac{z+u+1}{z+u-1}\right| + [1-(u-z)^2]\ln\left|\frac{z-u+1}{z-u-1}\right|\right] - \left[[1-(u-2z)^2]\ln\left|\frac{2z-u+1}{2z-u-1}\right| + [1-(u+2z)^2]\ln\left|\frac{2z+u+1}{2z+u-1}\right|\right]\right\}, \quad \text{(C12)}$$

$$\Sigma^C_{xxx}(2q;2\omega) = \frac{3ne^3u}{8m_e\hbar\omega^2 q}\left[(1-(u+z)^2)\ln\left|\frac{z+u+1}{z+u-1}\right| + (1-(u-z)^2)\ln\left|\frac{z-u+1}{z-u-1}\right| + 4z\right]. \quad \text{(C13)}$$

[1] V. V. Pavlov, G. Tessier, C. Malouin, P. Georges, A. Brun, D. Renard, P. Meyer, J. Ferre, and P. Beauvillain, Appl. Phys. Lett. **75**, 190 (1999).

[2] A. Kirilyuk, V. Kirilyuk, and T. Rasing, J. Magn. Magn. Mater. **198-199**, 620 (1999).

[3] N. N. Dadoenkova, I. L. Lyubchanskii, M. I. Lyubchanskii, and T. Rasing, Appl. Phys. Lett. **74**, 1880 (1999).

[4] T. Rasing, Appl. Phys. B: Lasers Opt. **68**, 477 (1999).

[5] T. V. Murzina, E. A. Ganshina, S. V. Guschin, T. V. Misuryaev, and O. A. Aktsipetrov, Appl. Phys. Lett. **73**, 3769 (1998).

[6] R. Carey, D. M. Newman, and M. L. Wears, Phys. Rev. B **58**, 14175 (1998).

[7] D. Budker, V. Yashchuk, and M. Zolotorev, Phys. Rev. Lett. **81**, 5788 (1998).

[8] M. Straub, R. Vollmer, and J. Kirschner, Phys. Rev. Lett. **77**, 743 (1996).

[9] T. Rasing, in *Notions and Perspectives of Nonlinear Optics*, edited by O. Keller (World Scientific, Singapore, 1996), pp. 339–369, ISBN 981-02-2627-6.

[10] T. Rasing, M. G. Koerkamp, B. Koopmans, and H. van der Berg, J. Appl. Phys. **79**, 6181 (1996).

[11] J. Reif, C. Rau, and E. Matthias, Phys. Rev. Lett. **71**, 1931 (1993).

[12] G. S. Agarwal, P. A. Lakshmi, J. P. Connerade, and S. West, J.

Phys. B **30**, 5971 (1997).
[13] *Nonlinear Optics in Metals*, edited by K. H. Bennemann (Oxford University Press, Oxford, 1998), ISBN 0-19-851893-5.
[14] A. K. Zvezdin and N. F. Kubrakov, Sov. Phys. JETP **89**, 77 (1999) [Zh. Eksp. Teor. Fiz. **116**, 141 (1999)].
[15] V. M. Arutunyan, G. G. Adonts, E. G. Kanetsian, and S. T. Hovsepian, Opt. Appl. **27**, 151 (1997).
[16] A. V. Petukhov, I. L. Lyubchanskii, and T. Rasing, Phys. Rev. B **56**, 2680 (1997).
[17] A. K. Zvezdin, Physica A **241**, 444 (1997).
[18] U. Pustogowa, W. Hübner, K. H. Bennemann, and T. Kraft, Z. Phys. B: Condens. Matter **102**, 109 (1997).
[19] A. Dähn, W. Hübner, and K. H. Bennemann, Phys. Rev. Lett. **77**, 3929 (1996).
[20] U. Pustogowa, T. A. Luce, W. Hübner, and K. H. Bennemann, J. Appl. Phys. **76**, 6177 (1996).
[21] W. Hübner, Phys. Rev. B **42**, 11553 (1990).
[22] J. P. Dewitz, J. Chen, and W. Hübner, Phys. Rev. B **58**, 5093 (1998).
[23] J. P. Dewitz and W. Hübner, Appl. Phys. B: Lasers Opt. **68**, 491 (1999).
[24] As pointed out by Landau and Lifshitz (see Ref. [25], p. 252). The properties of the multipolar expansion are discussed in detail in, e.g., Ref. [26] , Chap. 16. How to go beyond this long-wavelength approximation is discussed in, e.g., Refs. [27–30].
[25] L. D. Landau and E. M. Lifshitz, *Electrodynamics in Continuous Media* (Pergamon, New York, 1960).
[26] J. D. Jackson, *Classical Electrodynamics* (Wiley, New York, 1995), ISBN 0-471-43132-X.
[27] J. E. Sipe and G. I. Stegeman, *in Surface Polaritons*, edited by V. M. Agranovich and D. L. Mills (North-Holland, Amsterdam, 1982), pp. 661–701, ISBN 0-444-86165-3.
[28] A. Bagchi, R. G. Barrera, and A. K. Rajagopal, Phys. Rev. B **20**, 4824 (1979).
[29] P. J. Feibelman, Prog. Surf. Sci. **12**, 287 (1982).
[30] G. Mukhopadhyay and S. Lundqvist, Phys. Scr. **17**, 69 (1978).
[31] J. R. Ackerhalt and P. W. Milonni, J. Opt. Soc. Am. B **1**, 116 (1984).
[32] E. A. Power and S. Zienau, Philos. Trans. R. Soc. London, Ser. A **251**, 427 (1959).
[33] R. G. Woolley, Mol. Phys. **22**, 1013 (1971).
[34] L. Lorenz,K. Dan. Vidensk. Selsk., Mat.-Fys. Skr. **1**, 26 (1867); Pogg. Ann. **131**, 243 (1867); Philos. Mag. **34**, 287 (1867).
[35] O. Keller, in *Progress in Optics*, edited by E. Wolf (Elsevier, Amsterdam, 2002), Vol. 43, pp. 195–294, ISBN 0-444-51022-2.
[36] To study the behavior of electrons in an external electromagnetic field, the usual procedure (minimal coupling) is to replace $\mathbf{p}$ with $\mathbf{p}+e\mathbf{A}$ in the Dirac equation (see, e.g., Ref. [37], Chap. 1)
[37] S. Weinberg, *The Quantum Theory of Fields* (Cambridge, University Press, Cambridge, 1995).
[38] The magnetic field is usually written $\boldsymbol{B}=\boldsymbol{\nabla}\times\boldsymbol{A}$, but in this notation the curl operates only on the vector potential, not on the wave function, i.e., $\boldsymbol{B}\psi=\psi\boldsymbol{\nabla}\times\boldsymbol{A}$. In the notation $\boldsymbol{B}=\boldsymbol{\nabla}\times\boldsymbol{A}+\boldsymbol{A}\times\boldsymbol{\nabla}$, the nabla operator operates also on the wave function, i.e., $\boldsymbol{B}\psi=\boldsymbol{\nabla}\times(\boldsymbol{A}\psi)+\boldsymbol{A}\times\boldsymbol{\nabla}\psi$.
[39] E. Beaurepaire, J.-C. Merle, A. Daunois, and J.-Y. Bigot, Phys. Rev. Lett. **76**, 4250 (1996).
[40] T. V. Shahbazyan, I. E. Perakis, and J.-Y. Bigot, Phys. Rev. Lett. **81**, 3120 (1998).
[41] O. Keller, Phys. Rep. **268**, 85 (1996).
[42] O. Keller, Phys. Rev. B **33**, 990 (1986).
[43] Actually, in the integral form the expressions for the conductivities are valid also for finite temperature [at finite temperature one only has to replace the Heaviside unit-step function $\Theta(\cdots)$ with the Fermi-Dirac distribution function $f(\cdots)$] , since only in the integration step the low-temperature limit is taken.
[44] J. Lindhard, K. Dan. Vidensk. Selsk. Mat. Fys. Medd. **28**, No.8, 1 (1954).
[45] N. D. Mermin, Phys. Rev. B **1**, 2362 (1970).
[46] K. L. Kliewer, Surf. Sci. **101**, 57 (1980).
[47] L. V. Keldysh, D. A. Kirzhnitz, and A. A. Maradudin, *The Dielectric Function of Condensed Systems* (North-Holland, Amsterdam, 1989), ISBN 0-444-87366-X.
[48] O. Keller, Phys. Rev. B **43**, 10293 (1991).
[49] O. Keller, Mater. Sci. Eng., B **5**, 183 (1990).
[50] J. Friedel, Nuovo Cimento, Suppl. **7**, 287 (1958).
[51] T. Andersen, O. Keller, W. Hübner, and B. Johansson, Phys. Lett. A **320**, 465 (2003).
[52] By *direct conductivities* is meant that incoming electric fields are properly screened when they arrive at the relevant space points, i.e., the conductivities reflect the response to the local field, not the laser field. Similarly, the response is the local response, not the response at the site of the detector.
[53] N. W. Ashcroft and N. D. Mermin, *Solid State Physics* (Holt, Rinehart and Winston, New York, 1976), ISBN 0-03-083993-9.
[54] T. Andersen and O. Keller, Opt. Commun. **155**, 317 (1998).
[55] *754-1985 IEEE Standard for Binary Floating-Point Arithmetic 1985* (IEEE, New York, 1985), ISBN 1-5593-7653-8.
[56] D. M. Smith, ACM Trans. Math. Softw. **27**, 377 (2001); **24**, 359 (1998); **17**, 273 (1991).
[57] O. Keller, J. Opt. Soc. Am. B **16**, 835 (1999).
[58] Strictly speaking, by introducing electrons into the vacuum, the interactions between the electrons and photons gives rise to currents, creating a refractive index. Thereby the group velocity of the light differs from c_0 and thus, in general, in a homogeneous electron gas, $q \gtrsim q_0$.
[59] N. Bloembergen, R. K. Chang, S. S. Jha, and C. H. Lee, Phys. Rev. **174**, 813 (1968).
[60] A. Liu and O. Keller, Phys. Rev. B **49**, 13616 (1994).
[61] A. Liu and O. Keller, Phys. Scr. **52**, 116 (1995).
[62] T. Andersen and W. Hübner, Phys. Rev. B **65**, 174409 (2002).
[63] O. K. Andersen, Phys. Rev. B **12**, 3060 (1975).
[64] P. Blaha, K. Schwarz, G. Madsen, D. Kvasnicka, and J. Luitz, *WIEN2k, An Augmented Plane Wave Plus Local Orbitals Program for Calculating Crystal Properties* (Karlheinz Schwarz, Vienna, 2001), ISBN 3-9501031-1-2.
[65] N. Bloembergen, *Nonlinear Optics* (W. A. Benjamin, Reading, MA, 1965), ISBN 0-8053-0938-1.
[66] A. Messiah, *Quantenmechanik 2* (Walter de Gruyter, Berlin, 1990), ISBN 3-11-012669-9.
[67] T. Andersen and O. Keller, Phys. Rev. B **60**, 17046 (1999).
[68] In Eqs. (B17) and (B18), $n!!$ is the double factorial (e.g., $5!!=1\times3\times5$, and $8!!=2\times4\times6\times8$), and we have defined $0!!\equiv1$ and $(-1)!!\equiv1$, as usual.